AD-A164 357 DESIGN OF A SPACE BASED SENSOR TO PREDICT THE INTENSITY AND LOCATION OF EARTHQUAKES FROM ELECTROMAGNETIC RADIATION(U) NAVAL POSTGRADUATE SCHOOL MONTEREY CA 1/1

UNCLASSIFIED M L WHYMS DEC 85 F/G 8/11 NL

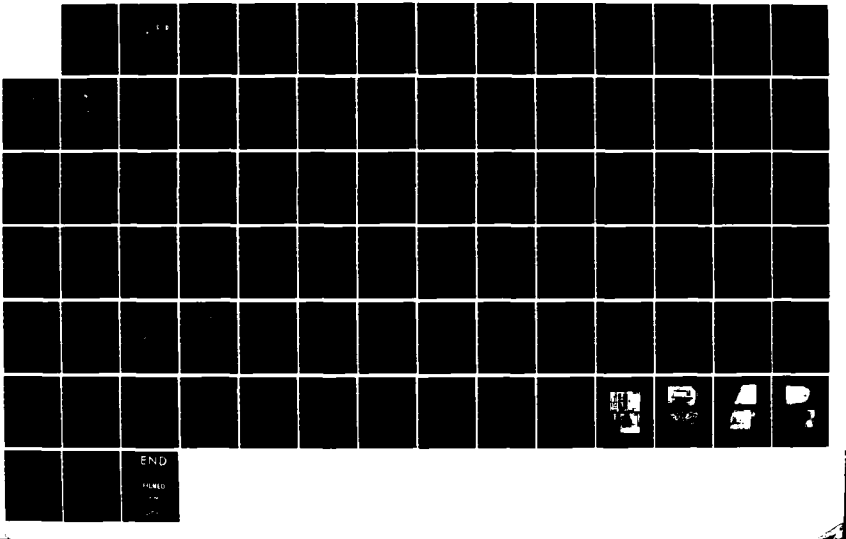

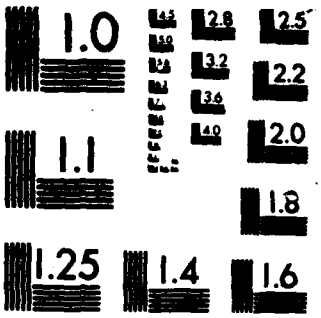

NAVAL POSTGRADUATE SCHOOL
Monterey, California

THESIS

DESIGN OF A SPACE BASED SENSOR TO PREDICT THE INTENSITY AND LOCATION OF EARTHQUAKES FROM ELECTROMAGNETIC RADIATION

by

Michael L. Whyms

December 1985

Thesis Advisor: R. W. Adler

Approved for public release; distribution is unlimited

SECURITY CLASSIFICATION OF THIS PAGE

AD-A164357

REPORT DOCUMENTATION PAGE

1a. REPORT SECURITY CLASSIFICATION	1b. RESTRICTIVE MARKINGS
2a. SECURITY CLASSIFICATION AUTHORITY	3. DISTRIBUTION/AVAILABILITY OF REPORT: Approved for public release; distribution is unlimited
2b. DECLASSIFICATION/DOWNGRADING SCHEDULE	
4. PERFORMING ORGANIZATION REPORT NUMBER(S)	5. MONITORING ORGANIZATION REPORT NUMBER(S)
6a. NAME OF PERFORMING ORGANIZATION: Naval Postgraduate School; 6b. OFFICE SYMBOL (If applicable): 62	7a. NAME OF MONITORING ORGANIZATION: Naval Postgraduate School
6c. ADDRESS (City, State, and ZIP Code): Monterey, California 93943-5100	7b. ADDRESS (City, State, and ZIP Code): Monterey, California 93943-5100
8a. NAME OF FUNDING/SPONSORING ORGANIZATION; 8b. OFFICE SYMBOL (If applicable)	9. PROCUREMENT INSTRUMENT IDENTIFICATION NUMBER
8c. ADDRESS (City, State, and ZIP Code)	10. SOURCE OF FUNDING NUMBERS: PROGRAM ELEMENT NO. / PROJECT NO / TASK NO / WORK UNIT ACCESSION NO.

11. TITLE (Include Security Classification)
DESIGN OF A SPACE BASED SENSOR TO PREDICT THE INTENSITY AND LOCATION OF EARTHQUAKES FROM ELECTROMAGNETIC RADIATION

12. PERSONAL AUTHOR(S)
Whyms, Michael L.

13a. TYPE OF REPORT	13b. TIME COVERED	14. DATE OF REPORT (Year, Month, Day)	15. PAGE COUNT
Master's Thesis	FROM _____ TO _____	1985 December	84

16. SUPPLEMENTARY NOTATION

17. COSATI CODES		
FIELD	GROUP	SUB-GROUP

18. SUBJECT TERMS (Continue on reverse if necessary and identify by block number)
Noise Measurement; Electromagnetic Radiation from Earthquakes, Space-Based Sensor

19. ABSTRACT (Continue on reverse if necessary and identify by block number)
A proposed design for a space-based sensor to predict and detect earthquakes is presented. A free standing radio frequency (RF) noise measurement and recording system is described to research the correlation between earthquakes and increased background electromagnetic noise at 30.45 MHz and 150.75 MHz.

20. DISTRIBUTION/AVAILABILITY OF ABSTRACT	21. ABSTRACT SECURITY CLASSIFICATION
☒ UNCLASSIFIED/UNLIMITED ☐ SAME AS RPT ☐ DTIC USERS	UNCLASSIFIED

22a. NAME OF RESPONSIBLE INDIVIDUAL	22b. TELEPHONE (Include Area Code)	22c. OFFICE SYMBOL
R. W. Adler	408-646-2352	62Ab

DD FORM 1473, 84 MAR — 83 APR edition may be used until exhausted. All other editions are obsolete.

SECURITY CLASSIFICATION OF THIS PAGE

Approved for public release; distribution is unlimited.

Design of a Space Based Sensor to Predict the Intensity and Location of Earthquakes from Electromagnetic Radiation

by

Michael L. Whyms
Lieutenant Commander, United States Navy
B.S., University of New Mexico, 1974

Submitted in par ial fulfillment of the requirements for the degree of

MASTER OF SCIENCE IN ELECTRICAL ENGINEERING

from the

NAVAL POSTGRADUATE SCHOOL
December 1985

Author: Michael L. Whyms
Michael L. Whyms

Approved by: R.W. Adler
R.W. Adler, Thesis Advisor

S. Jauregui Jr.
S. Jauregui Jr., Second Reader

Harriett B. Rigas
Harriett B. Rigas, Chairman,
Department of Electrical and Computer Engineering

John N. Dyer
John N. Dyer,
Dean of Science and Engineering

ABSTRACT

A proposed design for a space based sensor to predict and detect earthquakes is presented. A free standing radio frequency (RF) noise measurement and recording system is described to research the correlation between earthquakes and increased background electromagnetic noise at 30.45 MHz and 150.75 MHz.

TABLE OF CONTENTS

LIST OF TABLES

LIST OF FIGURES

ACKNOWLEDGEMENTS

I am deeply grateful to the numerous people who gave of their time freely and willingly in assisting me during the preparation of this thesis. Foremost, I wish to thank my wife whose encouragement and support allowed me to have the necessary time that was required for both the hardware development and thesis writing.

I also wish to express my gratitude to the Bullard Hall personnel, in particular ET1 John Babka who spent numerous hours and ceaseless energy in building and coordinating the construction of the electronic equipment. I also wish to thank Dr. Richard W. Adler and Dr. Stephen Jauregui, Jr., for providing technical support and guidance. Finally, I also wish to express my gratitude to the Electrical Shop of the Public Works Department for their valuable assistance and recommendations.

I. INTRODUCTION

A. EARTHQUAKE PREDICTION THEORY

The desirability of being able to predict when and where an earthquake will occur becomes immediately apparent in light of the recent devastation that occurred in Mexico City. The potential for death if a catastrophic earthquake should occur along the San Andreas fault is estimated to be between 3,000 and 13,000 lost lives. The lower figure applies for a quake that hits at 0230 and the higher figure applies for a quake that occurs at 1630 on a weekday. These predictions are based on the facts that wooden, single family homes are much more resistant to earthquake structural damage than are many of the older, unreinforced masonry buildings. In May, 1983, 30 of the 40 unreinforced masonry structures in Coalinga, Ca., either partially or totally collapsed. In Los Angeles, 8,000 similar buildings exist. The probability of a magnitude 8.3 earthquake occurring along the southern San Andreas fault within the next 30 years is estimated to be 50 percent. [Ref. 1:p. 35]

The primary cause of earthquakes is the movement of the lithosphere, the outer layer of the Earth consisting of twelve rigid plates riding on the supporting mantle. This movement rearranges continents and forms and destroys both mountains and oceans. The driving energy for this potentially large scale destructive mechanism is the convective circulation of the mantle. The mantle consists of hot, solid rock. In time measured on a geological scale, the mantle is sufficiently hot that it can flow and be easily deformed. Hot magma from the mantle wells up between separating plates at midocean ridges forming new lithosphere. The movement of the cold, brittle plates is primarily along boundary faults and is controlled by friction. Earthquakes

occur when these plates suddenly slip and elastically rebound. [Ref. 2]

Figures 1.1 and 1.2 [Ref. 1:p. 38] show the typical cycles of earthquakes as explained by the theory of plate tectonics. In figure 1.1 the hot mantle 10-15 km deep is plastically deforming and stress is accumulating at asperities, or lock points, in the cooler crust. At the moment of rupture an asperity breaks and crustal rupture spreads causing earthquakes. The slippage is halted when it encounters another asperity in approximately 100 seconds. Aftershocks may occur for the next several months. Additional slippage at or near the surface may or may not occur. In Figure 1.2 a second major earthquake has occurred 50 or 100 years after the first. The cycle begins again after about 200 years when the deep crust displacement imposes new stress on the upper brittle crust.

To date, earthquake prediction has been on a long-term basis normally expressed as a probability of quake occurrence during the coming scores of years. What has been lacking is a reliable, short-term prediction process. Central to any short-term technique is geologic phenomena during the period immediately preceding the main earthquake. Before the arrival of a major shock, swarms of many small earthquakes are often noted or sometimes accelerated deformation of the crust is observed. However, neither one of these two predictors is reliably present in all cases. [Ref. 1:p. 38]

Systematically collected data on the generation of electromagnetic energy prior to, during, or after an earthquake currently does not exist. Evidence of radio frequency (RF) emissions as a precursor to quake activity appears impulsively suggesting these waves are generated over a broad spectrum of frequencies [Ref. 3]. Citizen band and amateur radio operators in the Hollister, Ca., area reported an "increase in background noise level preceding earthquake

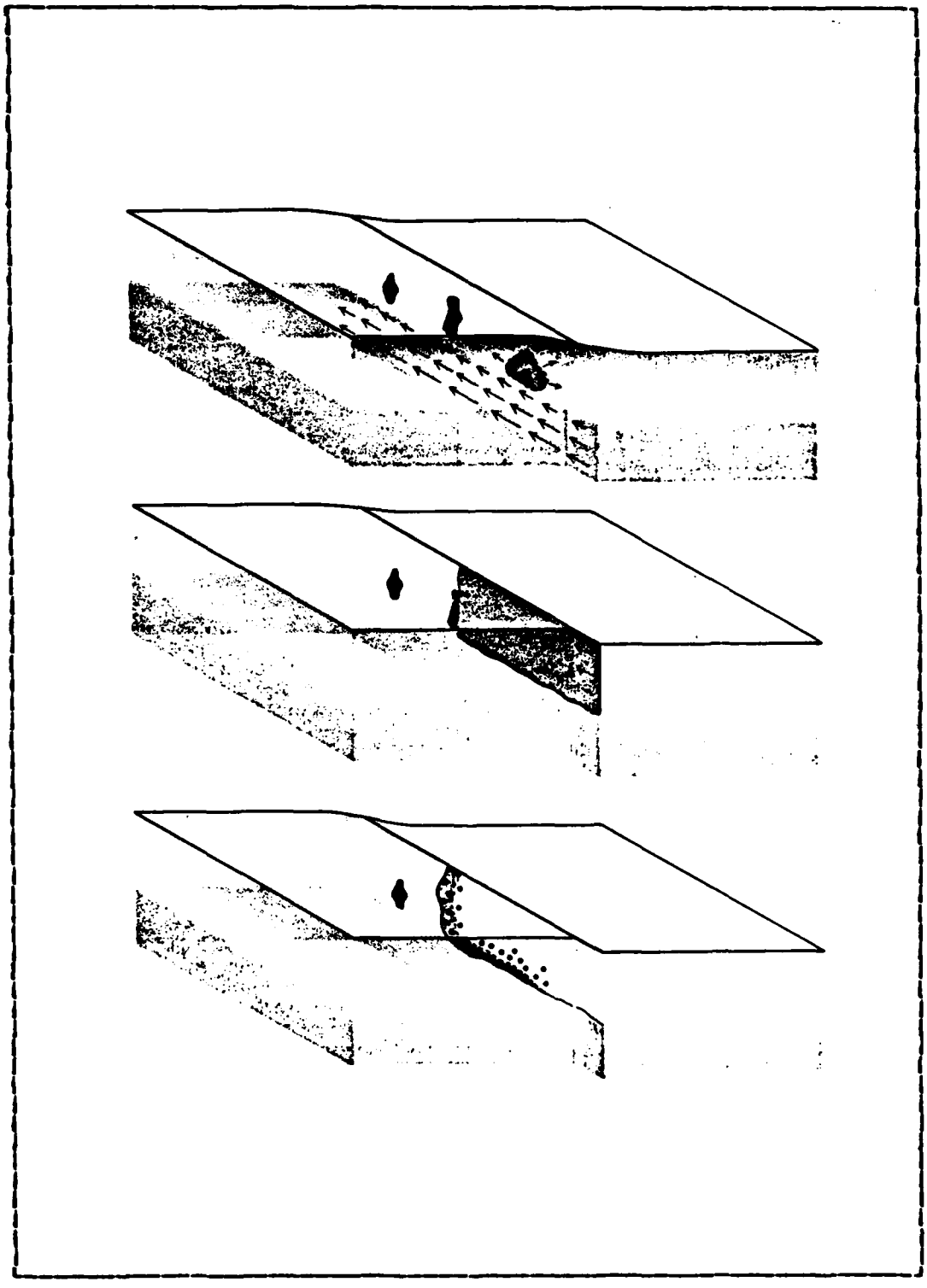

Figure 1.1 First Portion of an Earthquake Cycle

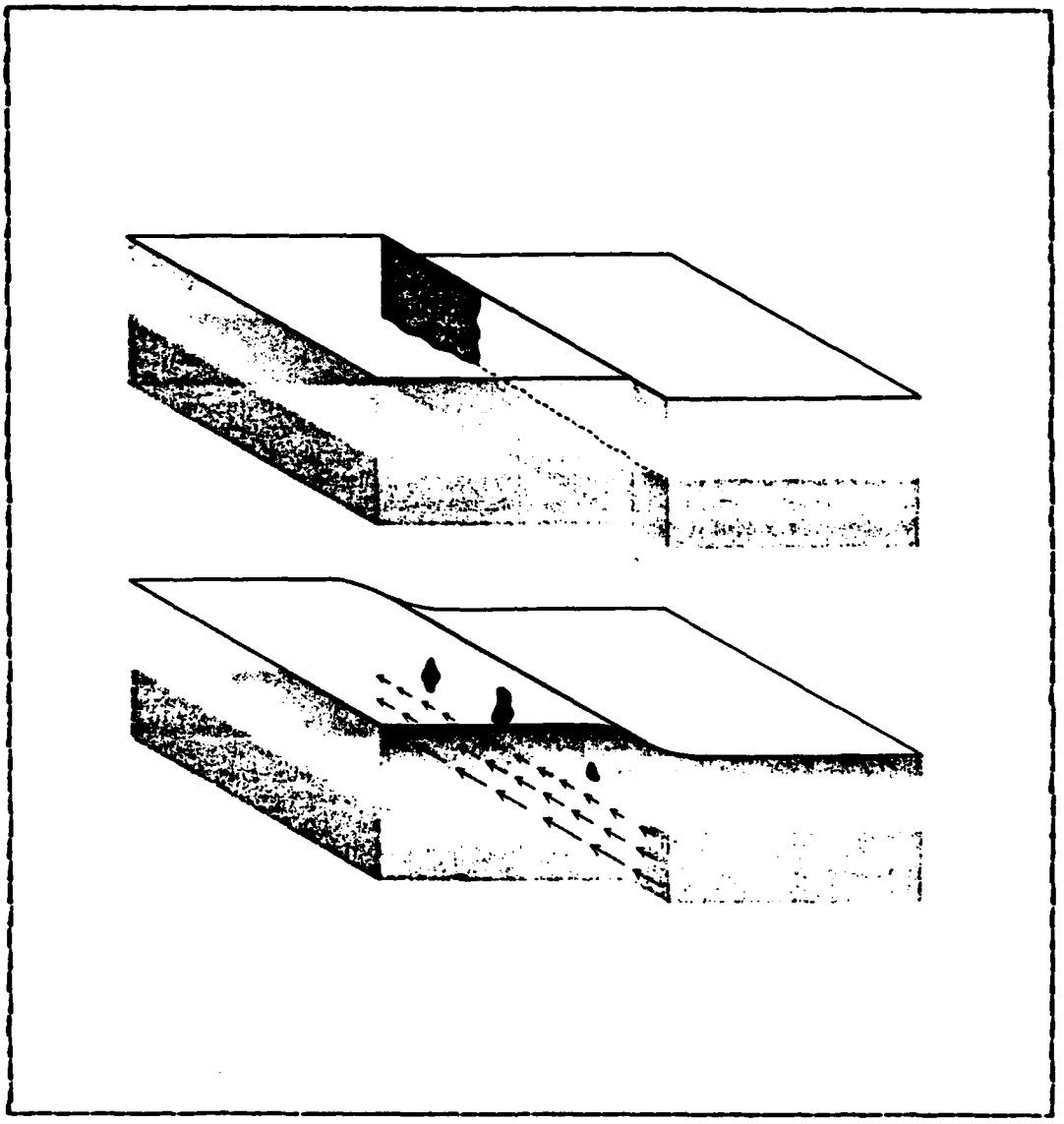

Figure 1.2 Second Portion of an Earthquake Cycle

activity" at 27 MHz and at the six and two meter bands. This increase in noise was on the order of 10 dB and preceded a quake by 12 to 24 hours. At one hour to 15 minutes before a quake, noise levels returned to normal. The appearance of earthquake lights [Ref. 4] and reception of 18 MHz radio noise [Ref. 5] are further examples of a possible connection between RF energy and earthquakes.

Various theories explaining the actual mechanism of RF generation at the fault boundary include impact of dissimilar metals, shock induced polarization and fracture of quartz-bearing rock [Ref. 6]. Because of the strong implication that earthquakes generate electromagnetic energy, this thesis will present a satellite design for a space-based system as a means of efficient quake detection and rapid data dissemination.

B. SPACE-BASED EARTHQUAKE DETECTION

The exploitation of outer space as a tool in earthquake prediction based on electromagnetic detection can be divided into two major scenarios. The first is installing ground-based sensors that detect the quake generated RF energy and then relay data to an orbiting satellite. The satellite would function as a central collection point and could incorporate features such as data processing and earthquake pattern recognition with automatic alarm transmission to key Earth stations. The number of ground-based sensors to provide adequate coverage can not be reliably estimated because the strength of the RF energy is not known but is being researched as a portion of this thesis. As the strength increases, the distance between sensors can increase and their number decrease.

The second scenario is direct detection of earthquake generated RF energy by an orbiting satellite. All the previously mentioned features could be included. Direct satellite detection would require a sufficiently strong RF signal to overcome the power spreading loss incurred from the large distance traveled. The major advantages over the first scenario are worldwide coverage with elimination of the need for ground-based RF sensors. On an international level, frequencies could be allocated to quake detection to minimize possible man-made interference with the RF signal. Because of the advantages, this second scenario will be the basis for the proposed satellite design.

C. FOCUS OF STUDY

A proposed design for a space based sensor to predict and detect earthquakes is presented. A free standing RF noise measurement and recording system is described to research the correlation between earthquakes and increased background electromagnetic noise at 30.45 MHz and 150.75 MHz. This thesis continues the research, construction and installation of equipment described in Reference 6.

II. BACKGROUND

A. ORBITAL PARAMETERS

1. Space Coordinate System

In order to understand the background information that will be used in subsequent portions of this thesis, it is necessary to first establish the coordinate system that describes a satellite's position in space. An ephemeris is a tabulation of the predicted or observed positions occupied by the satellite.

The coordinate system to be used is shown in Figure 2.1 [Ref. 7]. The large, flat rectangular plane is an extension of the plane of the equator and is called the equatorial plane. Superimposed on the equatorial plane is the Cartesian coordinate system indicated by $\overline{I}$, $\overline{J}$ and $\overline{K}$ with the origin at the Earth's center. These coordinates do not rotate but are fixed in space with the $\overline{I}$ axis pointing in the direction of the vernal equinox.

The satellite's motion about the Earth is on the circumference of the orbital plane. An elliptical orbit is shown but a satellite can also have a circular orbit around the Earth. The angular momentum or spin vector ($\overline{h}$) for the satellite orbit is determined by the right-hand rule for a south to north equator crossing and is perpendicular to the orbital plane. Inclination (i) is measured in degrees from $\overline{K}$ to the spin vector $\overline{h}$. By definition, inclination can vary from a minimum of zero degrees to a maximum of 180 degrees.

The eccentricity vector ($\overline{e}$) starts from the origin and points in the direction of perigee or the periapsis direction. Perigee is the satellite's closest point of approach to the Earth. The line of nodes ($\overline{n}$) is the intersection of the equatorial plane and the satellite's orbital plane. The angle between the line of nodes and the eccentricity vector is called the arguement of perigee and

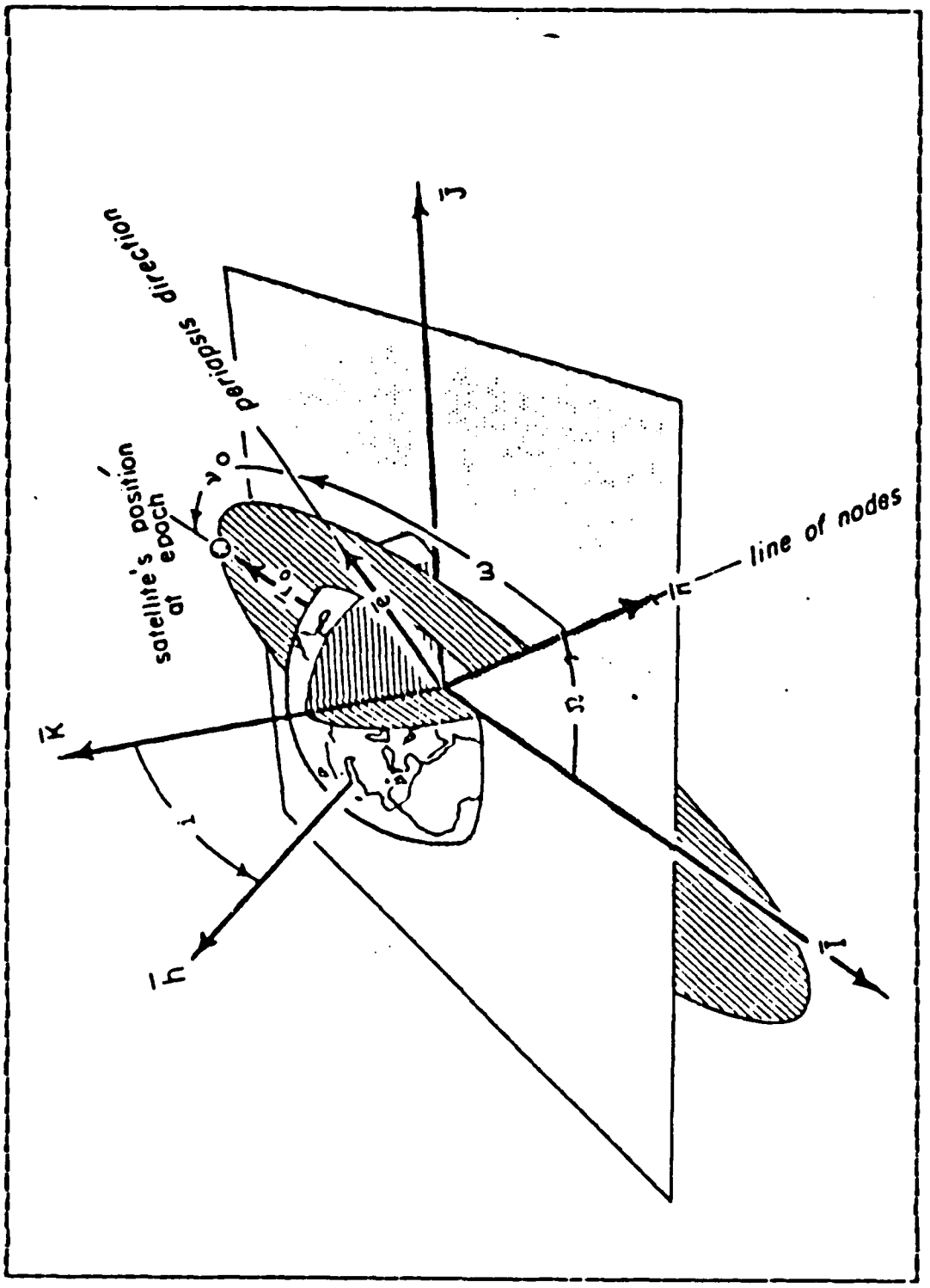

Figure 2.1 Classical Orbital Elements

is measured in the direction of the satellite motion. Right ascension of the line of nodes (Ω) is the angle measured in the equatorial plane from the vernal equinox direction to the line of nodes $\bar{n}$. The epoch angle (ν_0) is the angle measured from $\bar{e}$ to the vector from the center of the Earth to the satellite (r_0). The range of the epoch angle is from zero degrees to 360 degrees.

2. Equations for an Ellipse

Many satellites orbit the Earth in an elliptical manner or use portions of an elliptical orbit during an orbital transfer from one circular orbit to another circular orbit of a different radius. Because the equations of an ellipse are an integral portion of satellite orbitology, the pertinent relationships will be presented. Figure 2.2 shows the classical form of an ellipse with the small circle representing the Earth at one focus.

The semi-major axis (a) is the horizontal length measured from the center of the ellipse to the outer edge. The semi-minor axis (b) is the corresponding vertical length. The eccentricity (e) is a measure of departure from a circle and is given by Equation 2.1

$$e = SQRT(1-(b/a)^2) \qquad (2.1)$$

Eccentricity can vary from a value of zero indicating b = a for a circle to a value of slightly less than one if b approaches zero.

The radius of apogee (R_a) is the distance from the center of the Earth to the point of farthest distance from the Earth. The radius of perigee (R_p) is measured from the center of the Earth to the satellite's closest point of approach to the Earth. The relationship between R_a and e can be expressed as

$$R_a = a(1+e) \qquad (2.2)$$

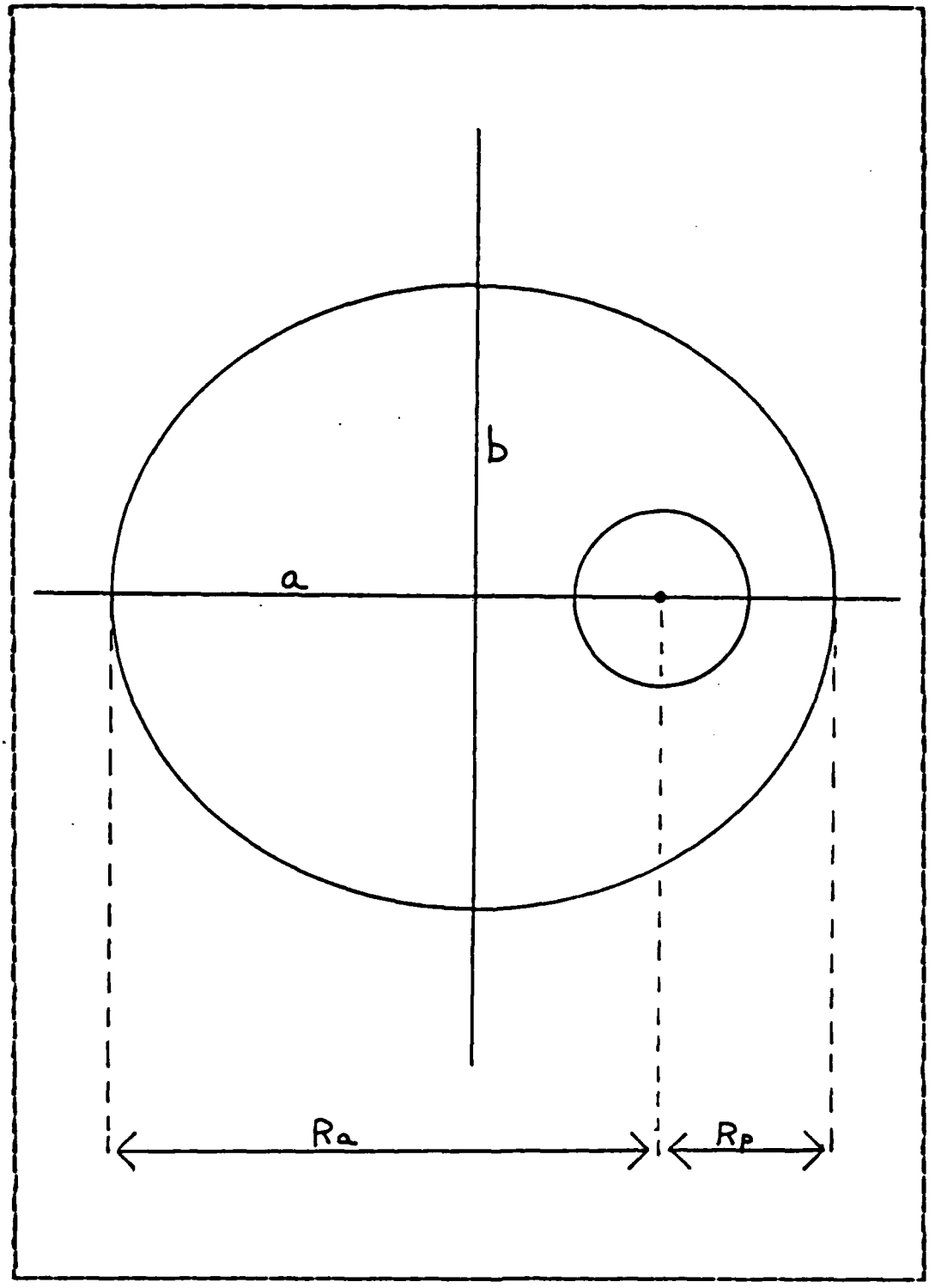

Figure 2.2 An Ellipse Around the Earth

A similar formula holds for R_p and e.

$$R_p = a(1-e) \tag{2.3}$$

B. ORBIT EQUATIONS

1. Circular and Elliptical Orbit Velocities

Two celestial bodies, one in orbit around the other, comprise a two-body system and must obey Newton's law of universal gravitation given by

$$F = \frac{GMm}{r^2} \tag{2.4}$$

Referring to Figure 2.3, F is the force of attraction due to gravity between masses M and m separated by a distance r. The constant G is the universal gravitational constant and its value is 6.67×10^{-11} $m^3/kg\ sec^2$. For any body of mass m in a circular orbit with velocity v and at a distance r, the centripital force is given by

$$F = \frac{mv^2}{r} \tag{2.5}$$

The centripital force must equal the gravitational force or the orbiting body will not be in an equilibrium orbit.

$$\frac{GMm}{r^2} = \frac{mv^2}{r} \tag{2.6}$$

Cancelling the common terms of m, one of the r's and solving for v yields

$$v = SQRT(GM/r) \tag{2.7}$$

This v is the linear velocity of mass m in a circular orbit about mass M at a radial distance r. The time required for

m to complete one circular revolution (T_c) is found by dividing the distance traveled ($2r\pi$) by the velocity. This gives

$$T_c = \frac{2r\pi}{V} \tag{2.8}$$

$$= \frac{2r\pi}{\text{SQRT}(GM/r)} \tag{2.9}$$

$$= \frac{2\pi r^{3/2}}{\text{SQRT}(GM)} \tag{2.10}$$

Kepler's third law of planetary motion relates the motion of one planet to another. This relationship is independent of the shape of their orbits and requires that the squares of the periods or the time to complete one revolution vary as the cubes of the semi-major axes. Then for m in an elliptical orbit about M with a semi-major axis of a, the time for one revolution (T_e) is given by

$$T_e = \frac{2\pi a^{3/2}}{\text{SQRT}(GM)} \tag{2.11}$$

The elliptical orbit velocity (V_e) is given by

$$V_e = \text{SQRT}[\,GM(2/r-1/a)\,] \tag{2.12}$$

2. Orbital Transfers

It is often desired to change the orbit of a satellite to place it either in a more advantageous relative position to other satellites or to alter its relative position to the Earth and allow it better access to Earth generated data. To perform an orbit modification the satellite must expend energy, normally in the form of burning fuel from an on-board rocket or releasing compressed gas through

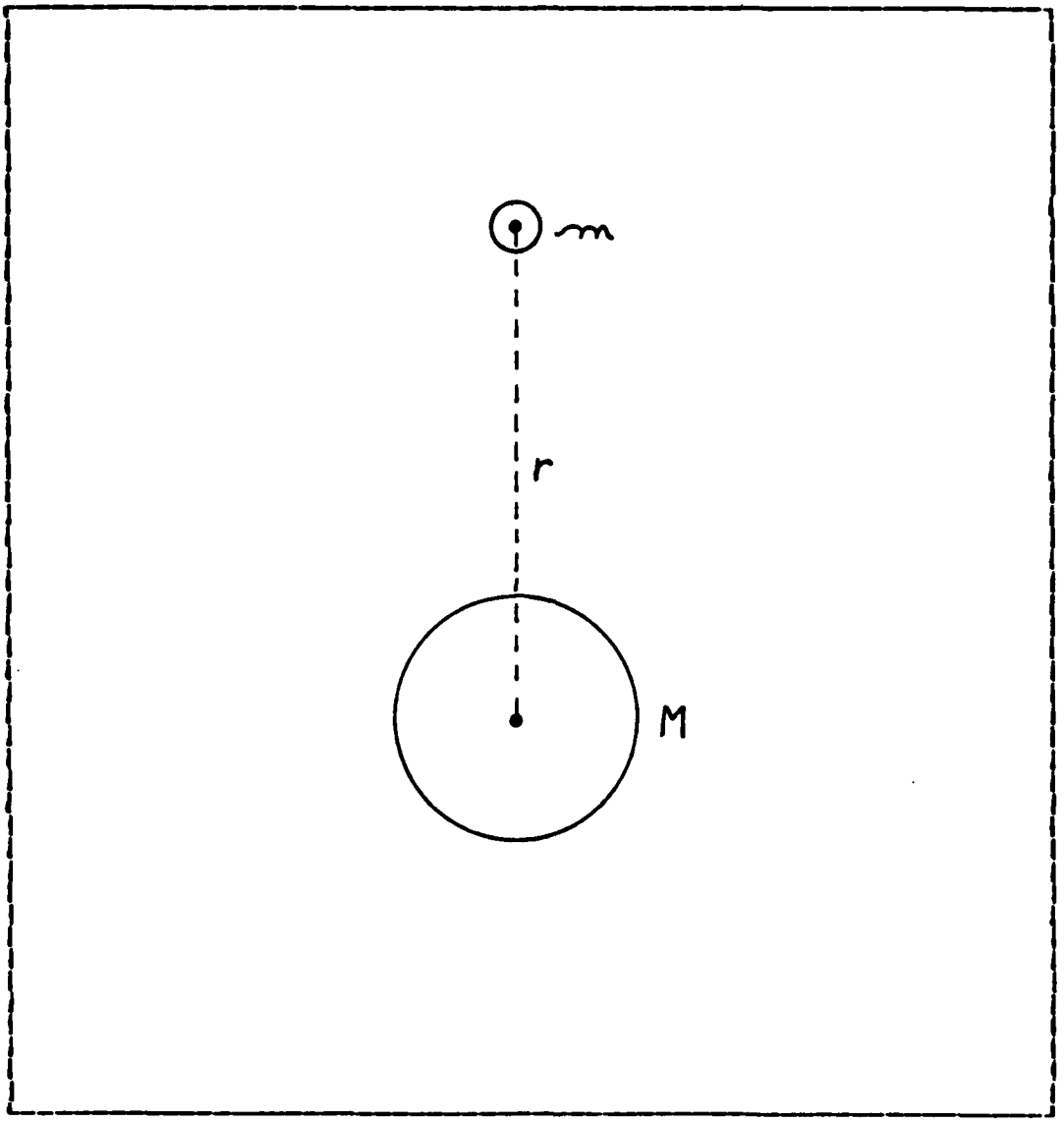

Figure 2.3 Gravitational Force of Attraction

thrusters. Rockets are used when a major change is desired because a large force can be quickly developed while compressed hydrazine gas powered thrusters are normally used for station keeping or very minor orbital adjustments.

The two major factors that influence exactly how an orbit modification will be accomplished are fuel and time. If it is desired to achieve the new orbit as rapidly as

possible, then a large amount of fuel will be required to provide the necessarily large force and acceleration. Such a time constraint may exist in the case of rescue missions or anti-satellite weapons. If time is not the deciding criterion then slower, more fuel efficient transfers are possible. This has the major advantage of allowing more of the satellite's weight to be in instrumentation since less weight need be allocated to fuel. A fuel efficient transfer will be used for this thesis to maximize operational payload.

Figure 2.4 depicts a satellite at position one in a counter-clockwise circular orbit about the Earth. It is desired to discharge a payload from the satellite so that upon completion of the maneuver, the payload will be in position two and the satellite will return to position one. The positions are separated by the angle u measured in radians. This same type of maneuver could be used if position one were to maneuver in order to rendezvous with a second satellite already at position two. To accomplish either task, the satellite at position one will accelerate into the elliptical orbit shown. While position two continues on its circular orbit and may pass the original position one several times, the accelerated satellite will travel the elliptical path and rendezvous will occur when both satellite one and two meet at position one. Note that the satellite at position one can not merely "speed up" to catch position two because by Equation 2.7 they would be at different distances from the Earth. It is necessary to know how much position one's velocity must be increased to place it into the correct elliptical orbit so rendezvous will occur.

Since the satellites are to meet at position one, the time for one elliptical orbit must be equal to the time for an integer number of circular orbits plus a portion of a circular orbit to account for the initial angular

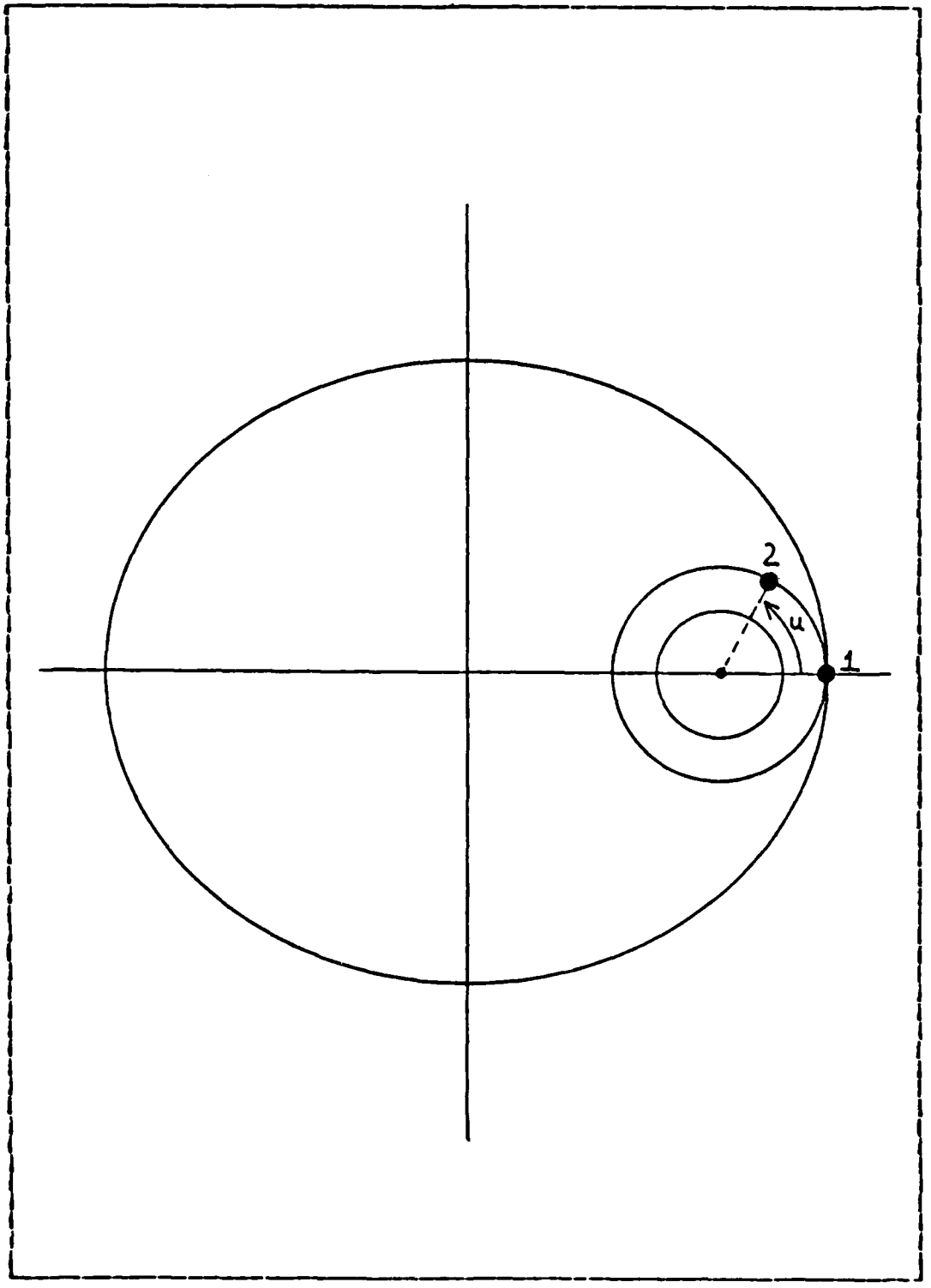

Figure 2.4 Circular Orbit Modification

difference. The integer number of orbits (K) can be selected to again either minimize time or fuel expended with more circular orbits indicating less fuel required. That is

$$KT_c + T_c(1-u/2\pi) = T_e \qquad (2.13)$$

Substituting Equations 2.10 and 2.11 into Equation 2.13 gives

$$\frac{K2\pi R_c^{3/2}}{SQRT(GM)} + \frac{2\pi R_c^{3/2}(1-u/2\pi)}{SQRT(GM)} = \frac{2\pi a^{3/2}}{SQRT(GM)} \qquad (2.14)$$

The circular orbit radius is now being represented by R_c rather than just r to assist in equation development. The common term of $2\pi/SQRT(GM)$ can be cancelled which leaves

$$KR_c^{3/2} + R_c^{3/2}(1-u/2\pi) = a^{3/2} \qquad (2.15)$$

Rearranging and solving for a gives

$$a = R_c[K+1-u/2\pi]^{2/3} \qquad (2.16)$$

Equation 2.16 gives an expression for a which is the semi-major axis of the required elliptical orbit. An expression is needed that relates the eccentricity of the transfer ellipse to K. This can be done by using Equation 2.3 and realizing that at perigee $R_c = R_p$. Making the substitution yields

$$a = a(1-e)[K+1-u/2\pi]^{2/3} \qquad (2.17)$$

Cancelling the a and rearranging gives

$$1 = [K+1-u/2\pi]^{2/3} - e[K+1-u/2\pi]^{2/3} \qquad (2.18)$$

Solving for e gives Equation 2.19

$$e = \frac{[K+1-u/2\pi]^{2/3} - 1}{[K+1-u/2\pi]^{2/3}} \qquad (2.19)$$

Equation 2.19 now relates the necessary eccentricity of the transfer ellipse to both the number of circular orbits of position two and to their initial angular separation. Equation 2.7 gives the circular orbit velocity and Equation 2.12 describes the elliptical orbit velocity. The velocity of the elliptical orbit at R_p must be known to find the difference between the two velocities. Evaluating Equation 2.12 at $r = R_p$ gives

$$V_p = SQRT[\, GM(2/R_p - 1/a)\,] \qquad (2.20)$$

V_p is the velocity at perigee for satellite one. Solving Equation 2.3 for a gives

$$a = \frac{R_p}{1-e} \qquad (2.21)$$

Substituting Equation 2.21 into Equation 2.20 and simplifying yields

$$V_p = SQRT[\, (GM/R_p)\,(1+e)\,] \qquad (2.22)$$

The required change in velocity can now be computed by subtracting V_c from V_p.

$$V_p - V_c = SQRT[\, (GM/R_p)\,(1+e)\,] - SQRT[\, GM/R_c\,] \qquad (2.23)$$

At perigee $R_c = R_p$; V_{pc} will represent the difference in velocity.

$$V_{pc} = SQRT(GM/R_c)[\, SQRT(1+e) - 1] \qquad (2.24)$$

The square root of (1 + e) can be approximated by

$1 + .5e + \ldots$. Also note that $SQRT(GM/R_c) = V_c$. Thus Equation 2.24 can be written as

$$V_{pc} = V_c[1 + .5e - 1] \tag{2.25}$$

$$= \frac{V_c e}{2} \tag{2.26}$$

$$= \frac{V_c[(K+1-u/2\pi)^{2/3} - 1]}{2[K+1-u/2\pi]^{2/3}} \tag{2.27}$$

Equation 2.27 is a key formula and can be used to determine how much additional velocity is required to ensure a proper rendezvous transfer orbit. It has the flexibility to vary the number of circular orbits which is equivalent to being able to predetermine the rendezvous time.

The use of this equation can be extended to deploying numerous, equally spaced satellites from a single large parent vehicle. The parent vehicle would be in the elliptical orbit carrying the satellites to be deployed. Each time the "rendezvous point" is achieved a satellite would be ejected. Two satellites would not be placed in the same position as the new rendezvous point is always u radians ahead of the current one. Because Equation 2.27 has u as a variable parameter, any angular positioning is possible and numerous satellites may be deployed limited only by the total weight that can be launched from Earth.

3. Orbital Transfer Fuel Requirements

The next parameter that must be calculated is how much fuel is required to inject the parent satellite from the circular orbit into the elliptical orbit. Comparison of Equations 2.7 and 2.22 show that V_p has a larger magnitude than V_c even though both are at a distance R_p from the center of the Earth. Thus, a transfer from a circular to

elliptical orbit requires the satellite to accelerate in the direction of travel. Similarly, when the parent satellite ejects a payload, that payload must burn fuel and slow down to V_c or it would continue on the parent's elliptical path. The amount of fuel required for either maneuver is critical since not only the fuel but also its container subtract from the weight that could be used for instrumentation.

Rocket fuel energy is classified by its specific impulse (I_{sp}) and is a measure of the thrust developed as a function of fuel mass flow rate. The mass flow rate can be in terms of gallons per minute for a liquid fuel or pounds per second for a burning solid fuel. The accepted English units for I_{sp} are expressed as seconds. This comes from

$$I_{sp} = \frac{\text{pounds of thrust}}{\text{pounds of fuel/second}} = \text{seconds} \qquad (2.28)$$

Typical values of I_{sp} range from 275-325 seconds. Knowing the fuel I_{sp}, the force of acceleration or thrust (F_t) can be found by

$$F_t = I_{sp}(dW/dt) \qquad (2.29)$$

W is the propellent weight flow rate.

The rocket thrust is generated from burning fuel that exits the rocket at a velocity V_x with units of feet per second. The fuel I_{sp} and exhaust velocity can be related by

$$V_x = gI_{sp} \qquad (2.30)$$

where g is the acceleration constant equal to 32.2 ft/sec^2. The thrust can also be related to the exhaust velocity and fuel flow rate by

$$F_t = -(dm/dt)V_x \qquad (2.31)$$

The minus sign is necessary because the exhaust is traveling in one direction and the resultant force is in the opposite direction. By Newton's laws, the rocket must react to the fuel thrust by

$$F = M_s a \tag{2.32}$$

M_s is the mass of the rocket being accelerated and a is the resultant acceleration. The acceleration can be written in terms of the rocket velocity (V_r) as

$$a = dV_r/dt \tag{2.33}$$

Substituting Equation 2.33 into Equation 2.32 gives

$$F = M_s (dV_r/dt) \tag{2.34}$$

F_t must equal F. Setting Equation 2.34 equal to Equation 2.31 gives

$$M_s (dV_r/dt) = -(dm/dt) V_x \tag{2.35}$$

Simplifying and rearranging terms gives

$$dV_r = -V_x (dm/M_s) \tag{2.36}$$

The left side of this equation can now be integrated from the initial rocket velocity (V_i) to the final rocket velocity (V_f). The right side can be integrated from the initial rocket weight (W_i) to the final rocket weight (W_f).

$$\int_{V_i}^{V_f} dV_r = -V_x \int_{W_i}^{W_f} \frac{dM_s}{M_s} \tag{2.37}$$

Equation 2.38 shows the evaluation result.

$$V_f - V_i = -V_x \ln(W_f / W_i) \quad (2.38)$$

Dividing by $-V_x$ and using both sides as a power of the exponential e gives

$$\exp[-(V_f - V_i)/V_x] = W_f / W_i \quad (2.39)$$

$$W_f = W_i \exp[-(V_f - V_i)/V_x] \quad (2.40)$$

The initial weight must be the sum of the final weight plus the weight of any fuel or propellent that was burned (W_p) to produce the change in velocity, or

$$W_f = W_i - W_p \quad (2.41)$$

Substituting Equation 2.41 into Equation 2.40 gives

$$W_i - W_p = W_i \exp[-(V_f - V_i)/V_x] \quad (2.42)$$

Solving for W_p gives

$$W_p = W_i [1 - \exp-(V_f - V_i)/V_x] \quad (2.43)$$

Replacing V_x with gI_{sp} from Equation 2.30 gives

$$W_p = W_i [1 - \exp-(V_f - V_i)/(gI_{sp})] \quad (2.44)$$

The quantity $V_f - V_i$ is the same change in velocity required by Equation 2.27 for orbital transfer.

$$V_{pc} = V_f - V_i \quad (2.45)$$

Equation 2.44 then becomes

$$W_p = W_i[\,1 - \exp-(V_{pc}/gI_{sp})\,] \qquad (2.46)$$

Equation 2.27 can be used to determine the amount of velocity change that is needed for an orbital transfer and Equation 2.46 is used to determine the percentage of initial satellite weight that must be reserved for the fuel to accomplish the same transfer.

III. SATELLITE DESIGN

A. GENERAL DESIGN

The satellite will be placed in a circular low Earth orbit (LEO) of 322 km. An orbit close to the Earth will be used because of the anticipated low power level of the earthquake electromagnetic signal. The design of the satellite will be based on using the space shuttle for achieving the initial circular orbit. Because of the large cargo bay on the shuttle (60 ft X 15 ft), a group of four satellites arranged in a circle and mounted on a central support bus will comprise the launch package. When deployed, the satellites will be equally spaced by 90 degrees.

Primary electrical power will be provided by solar cells with batteries supplying power during the time the satellite is in the Earth's shadow. Spin stabilization of the satellite body with hydrazine thrusters for station keeping will be used to maintain a de-spun antenna pointing at the Earth with attitude sensing to be done by Earth limb sensors. Each satellite will weigh approximately 500 pounds and have a cylindrically shaped main body.

B. ANTENNA DESIGN

The satellite will be designed to detect electromagnetic energy in the 30 MHz region. This frequency is used because it is designated for astronomical observations and manmade interference should be at a minimum. Additionally 30 MHz is well above the cutoff frequency (F_p) for propagation through the ionosphere given by

$$F_p = 9\,\mathrm{SQRT}(N_e) \qquad (3.1)$$

where N_e is the ionospheric plasma electron density with units of electrons/meter^3. A nominal value for F_p is

10 MHz. Any frequency higher than F_p will successfully penetrate into outer space with lower frequencies being reflected back to Earth.

A Yagi antenna will be used as the main sensor because of the size and space constraints imposed by a satellite design. Reference 8 will be used as a basis for the design of the antenna. Table I [Ref. 8:p. 7] is used once the initial design criteria is established. This initial data consists of the frequency of operation (30 MHz), antenna gain desired (9.2 dB), d/λ ratio where d is the diameter of the parasitic elements (2 cm), and the D/λ ratio where D is the diameter of the support boom (4 cm). The wavelength λ is given by

$$\lambda = \frac{c}{f} \tag{3.2}$$

The speed of light (c) is a constant equal to 3×10^8 meters/second and f is the operating frequency. Thus a frequency of 30 MHz gives a wavelength of 10 meters. Following the steps in Reference 8, Figure 3.1 [Ref. 8:p. 20] gives the length of the first and third director as 4.44 meters, 4.5 meters for the length of the second director and 4.9 meters for the length of the reflector. The element spacing is 2 meters. Deployment of the antenna in outer space can be achieved by using a bistem which is a deployable boom rolled up on a drum in its flattened configuration. Because of its small size when stowed, total storage space required will be approximately one-half a cubic foot. Since the antenna will be operating in a weightless environment, strong structural members are not required. The total weight of the antenna would not exceed 30 pounds since the material of construction could be a light-weight aluminum based alloy. The gain of 9.2 dB is referenced to a dipole antenna. For reference to an isotropic radiator, 2.16 dB of gain must be added.

TABLE I

YAGI ELEMENT LENGTHS

		LENGTH OF YAGI IN WAVELENGTHS					
		0.4	0.8	1.20	2.2	3.2	4.2
LENGTH OF REFLECTOR, λ		0.482	0.482	0.482	0.482	0.482	0.475
LENGTH OF DIRECTOR, λ	1st	0.424	0.428	0.428	0.432	0.428	0.424
	2nd		0.424	0.420	0.415	0.420	0.424
	3rd		0.428	0.420	0.407	0.407	0.420
	4th			0.428	0.398	0.398	0.407
	5th				0.390	0.394	0.403
	6th				0.390	0.390	0.398
	7th				0.390	0.386	0.394
	8th				0.390	0.386	0.390
	9th				0.398	0.386	0.390
	10th				0.407	0.386	0.390
	11th					0.386	0.390
	12th					0.386	0.390
	13th					0.386	0.390
	14th					0.386	
	15th					0.386	
SPACING BETWEEN DIRECTORS, IN λ		0.20	0.20	0.25	0.20	0.20	0.308
GAIN RELATIVE TO HALF-WAVE DIPOLE IN dB		7.1	9.2	10.2	12.25	13.4	14.2
DESIGN CURVE		(A)	(B)	(B)	(C)	(B)	(D)

C. FUEL REQUIREMENTS

1. Satellite Fuel

The on-station weight of the satellite is 500 pounds and this weight must be decelerated from the parent's elliptical velocity. Equation 2.27 will be used to determine the necessary velocity change and Equation 2.7 will be used to find V_c. GM evaluates as a constant equal to 3.99×10^{14} m^3/sec^2 and r is the sum of the radius of the Earth (6370 Km) and the satellite altitude above the Earth (322 Km).

$$V_c = SQRT(3.99 \times 10^{14}/6692 \times 10^3) \quad (3.3)$$

$$= 7{,}722 \text{ m/sec} \quad (3.4)$$

$$= 25{,}335 \text{ ft/sec} \quad (3.5)$$

Equation 2.27 can now be evaluated if K is set equal to one and u is set equal to $\pi/2$ radians.

$$V_{pc} = \frac{25{,}335[(2-.25)^{2/3} - 1]}{2[(2-.25)^{2/3} - 1]} \quad (3.6)$$

$$= 3{,}945 \text{ ft/sec} \quad (3.7)$$

Equation 2.46 can be used to find the fuel fraction given by

$$W_p/W_i = 1 - \exp-[3945/(32)(300)] \quad (3.8)$$

$$= .337 \quad (3.9)$$

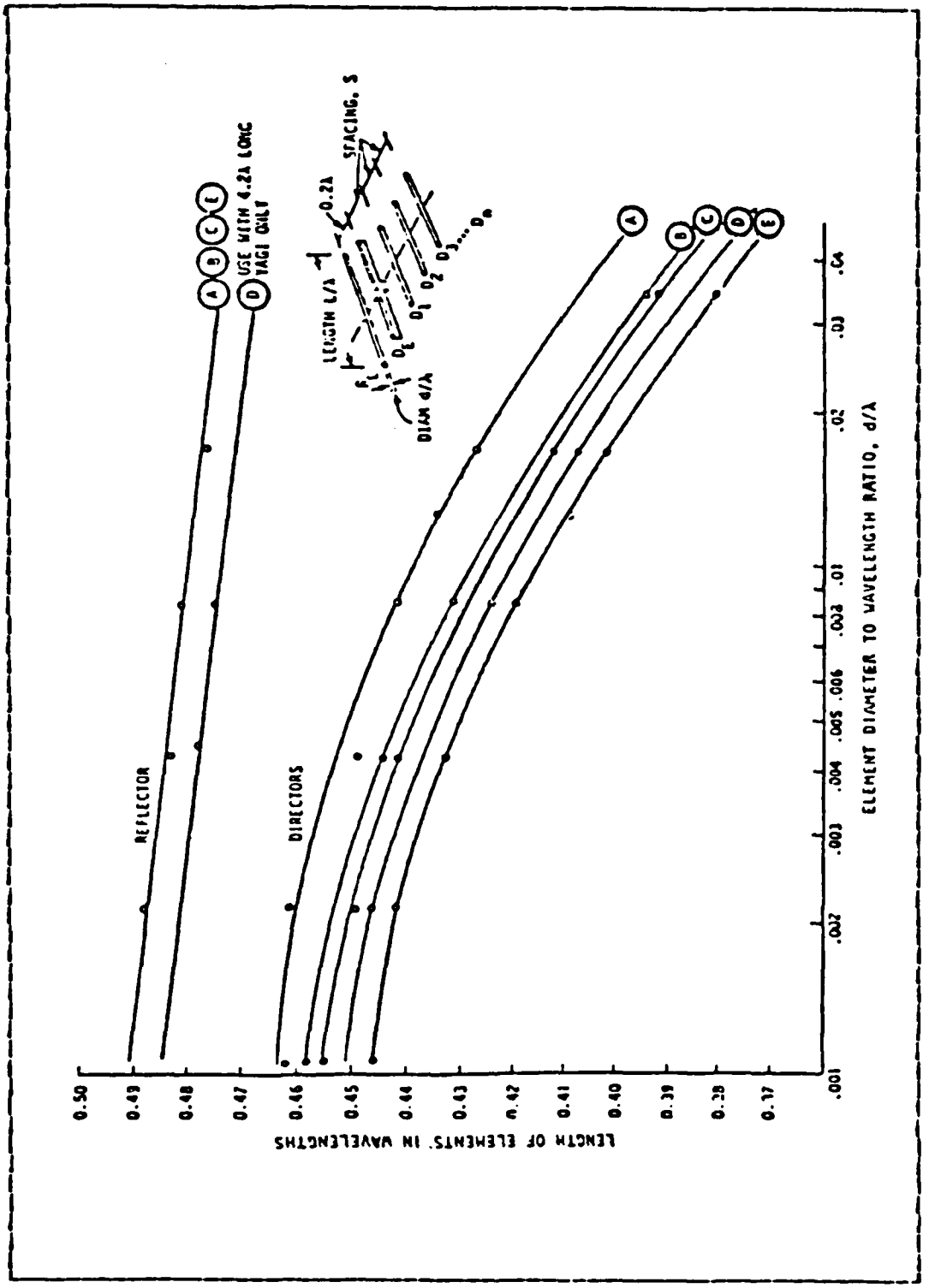

Figure 3.1 Yagi Antenna Design Curves

The initial weight is composed of the on-orbit satellite weight of 500 pounds (W_s), W_p and the weight of the case (W_c) that contains the fuel. That is

$$W_i = W_s + W_p + W_c \tag{3.10}$$

For an efficiently designed rocket motor, the majority of the weight is due to fuel with the remaining weight due to the case. This ratio (f) is given by

$$f = \frac{W_p}{W_p + W_c} \tag{3.11}$$

A typical value of f is 0.93. Using this definition of f, Equation 3.10 can be rewritten as

$$W_i = W_s + W_p/f \tag{3.12}$$

Substituting $W_p = .337W_i$ from Equation 3.9 and 0.93 for f into Equation 3.12 gives

$$W_i = W_s + .337W_i/.93 \tag{3.13}$$

Rearranging terms to solve for W_i and substituting 500 pounds for W_s gives

$$W_i = \frac{500}{1 - .337/.93} \tag{3.14}$$

$$= 784 \text{ lb} \tag{3.15}$$

This can be used to find W_p from Equation 3.9

$$W_p = (784)(.337) \tag{3.16}$$

$$W_p = 264 \text{ lb} \tag{3.17}$$

The weight of the case can be found by rearranging Equation 3.11

$$W_c = \frac{W_p(1-f)}{f} \tag{3.18}$$

$$= \frac{264(1-.93)}{.93} \tag{3.19}$$

$$= 20 \text{ lb} \tag{3.20}$$

2. Parent Satellite Fuel

The amount of fuel required by the parent to inject itself into the elliptical orbit can now be calculated in a similar manner. The central support bus weight will be set at 500 pounds. This relatively large weight is required because the bus must be strong enough to rigidly hold the four satellites during the shuttle launch. Thus, enough fuel must be allowed to accelerate the bus and three satellites into an elliptical orbit since one satellite is deployed prior to the parent's acceleration. The net weight to be boosted is then 2,852 pounds. Similar to Equation 3.14, the initial total weight is

$$W_i = \frac{2852}{1 - .337/.93} \tag{3.21}$$

$$= 4,473 \text{ lb} \tag{3.22}$$

The fuel weight and case weight for the parent can also be found in the same manner as for the individual satellite.

$$W_p = (4473)(.337) \tag{3.23}$$

$$W_p = 1{,}507 \text{ lb} \tag{3.24}$$

$$W_c = \frac{1507(1-.93)}{.93} \tag{3.25}$$

$$= 114 \text{ lb} \tag{3.26}$$

D. ELECTRICAL POWER

The primary source of electrical power will be provided by converting light energy into electrical energy by use of solar cells. Because the available power from an individual cell is small (on the order of 0.06 watts), a large number of cells must be used that collects solar energy over a large incident area. In order to provide the desired total power at useful voltages, solar cell configurations are normally used in a series-parallel connection.

The satellite will not be in sunlight during the Earth-Sun eclipse periods of the orbit. During these times, rechargeable batteries will provide the electrical power. Additionaly, the batteries can provide back-up power during transients that exceed the solar panel capacity.

In order to provide a useful power system, these two power sources must be integrated with a power control and power conversion system. Functions that must be accomplished include battery charging during sunlight periods, bus voltage monitoring and control and converting battery power to electrical power when required.

Figure 3.2 [Ref. 9:p. 1-7.5] shows a block diagram of a satellite power system. While only one of each component is shown, normal installations consist of multiple components for reliability reasons. The power from the main solar panel supplies the spacecraft systems through the primary power distribution bus. The output voltage of the panel can

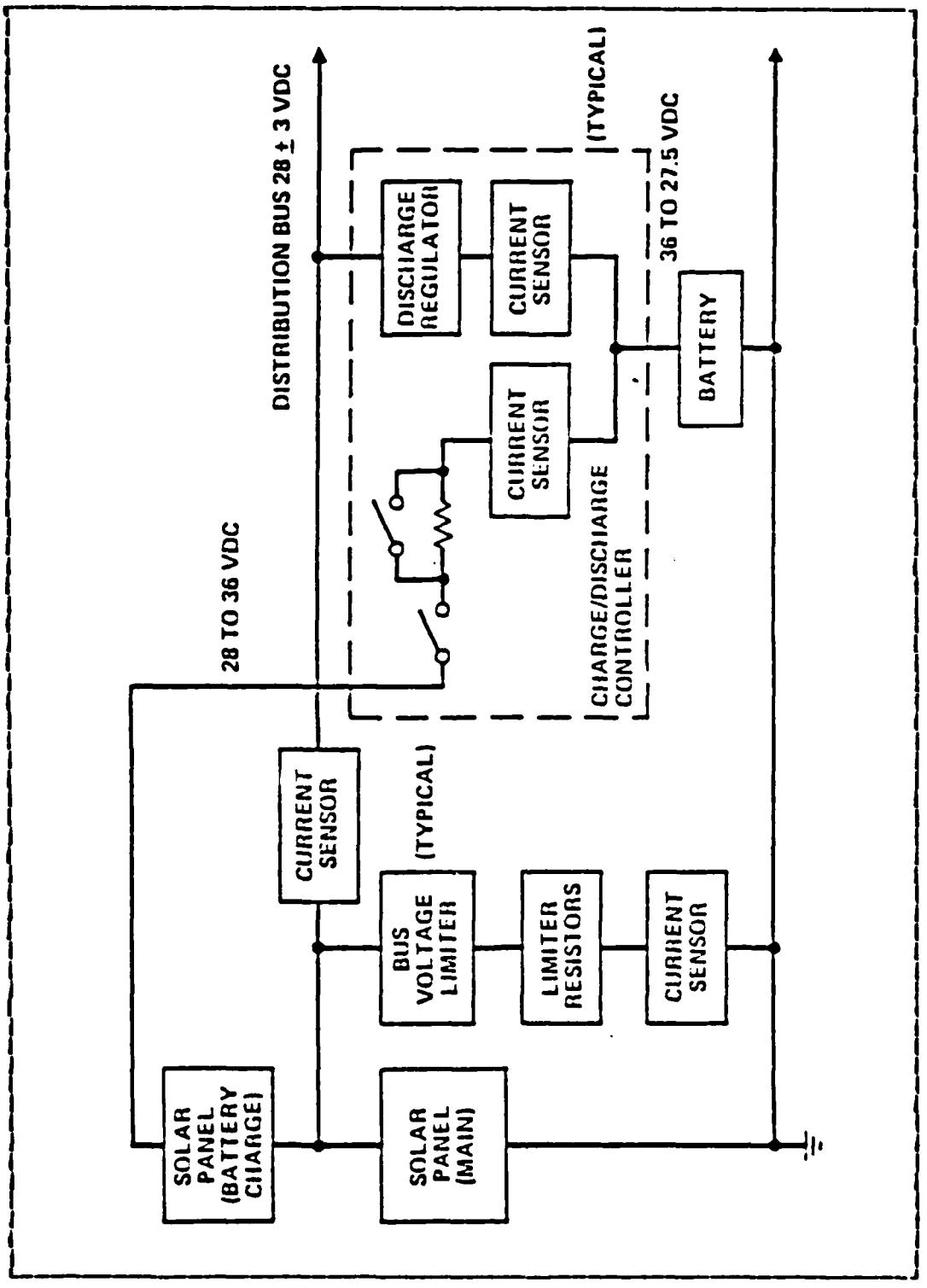

Figure 3.2 Satellite Power System

vary as a function of load, temperature and other factors. Bus voltage limiters prevent the voltage swings from exceeding spacecraft design ranges by acting as variable shunt loads during a rising voltage condition. The battery discharge regulator turns on when a pre-determined bus low voltage is sensed and provides a regulated output. The battery terminal voltage is higher than the required bus voltage and in order to charge the battery a still higher level of voltage is needed. To provide this higher voltage level, the additional solar panel is series connected to the main panel. The size of the battery charging panel is designed so that the charge control functions provided in the controller need only be an on-off and rate change switch. The voltage and current sensors provide means to monitor the operational state of the power system and for load managing during the orbit.

1. Solar Panel Design

As shown in Figure 3.3 [Ref. 9:p. 1-7.11] individual solar cells are arranged in a series-parallel array to provide the required power. The three strings are in parallel to minimize power loss should a single cell fail. These arrays are mounted on the satellite with the series string length parallel to the satellite spin axis. All the arrays are then connected in parallel to produce the desired power. The surface of the solar cell is considered to be a Lambertian surface and the power produced by the cell decreases by a cosine function as the sun's incident angle changes from normal as shown in Figure 3.4 [Ref. 9:p. 1-7.11].

Figure 3.5 [Ref. 9:p. 2-4.17] shows how the sun's incident angle varies during one year. When the solar cells are in the sunlight, only those positioned in the center are illuminated by normal rays. Going left or right from center causes the cell output to drop by the cosine function. The net result is an output from the half-cylinder that is equal

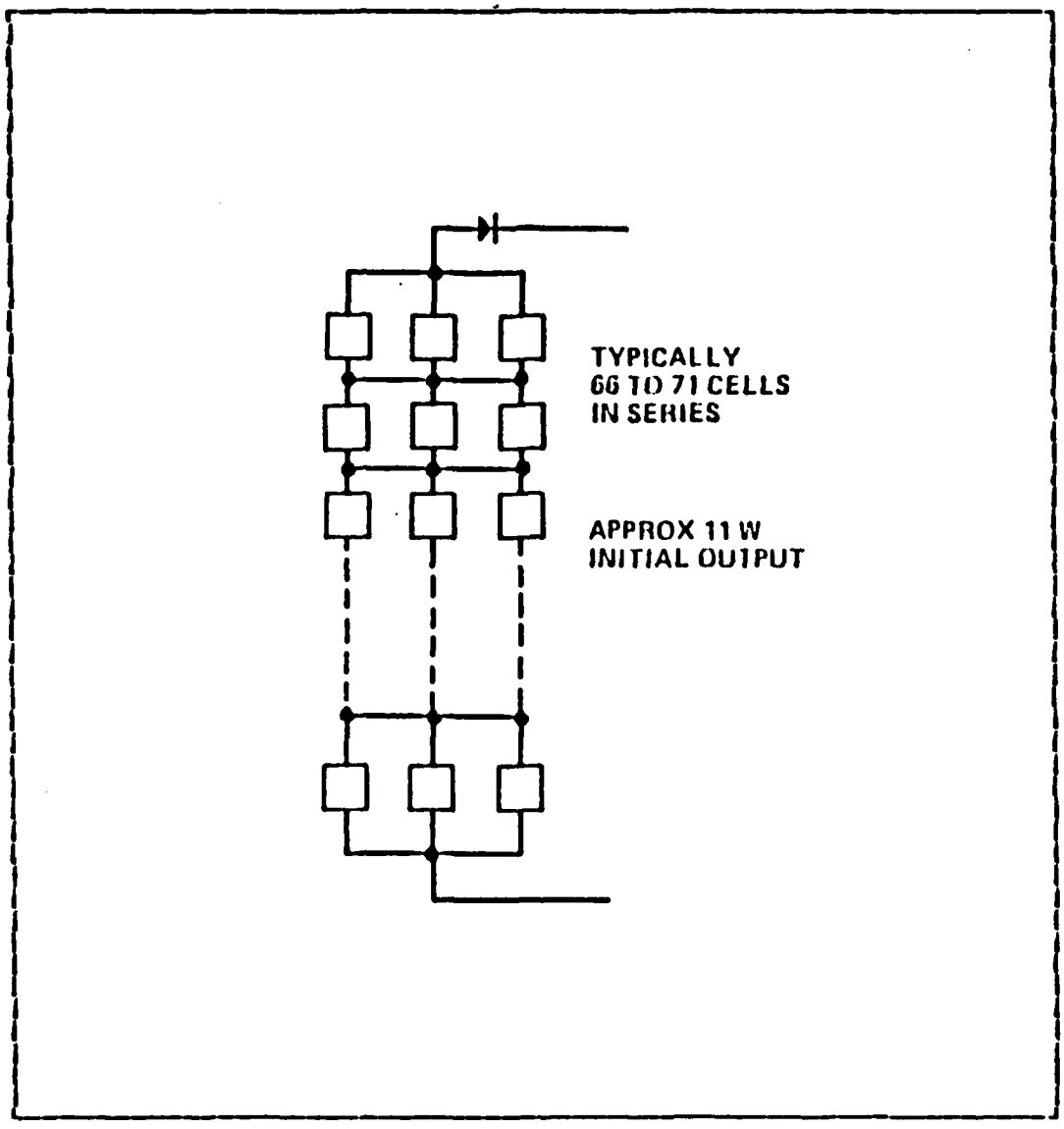

Figure 3.3 Solar Cell Array

to the output from a flat plate whose dimensions are the diameter and height of the cylinder. Additionally, the sun line varying 23.5 degrees as shown in Figure 3.5 causes a further decrease in solar panel output power.

Solar cell performance also degrades with time from exposure to electron and proton fields trapped in the Earth's magnetic field and solar flares. The extent of

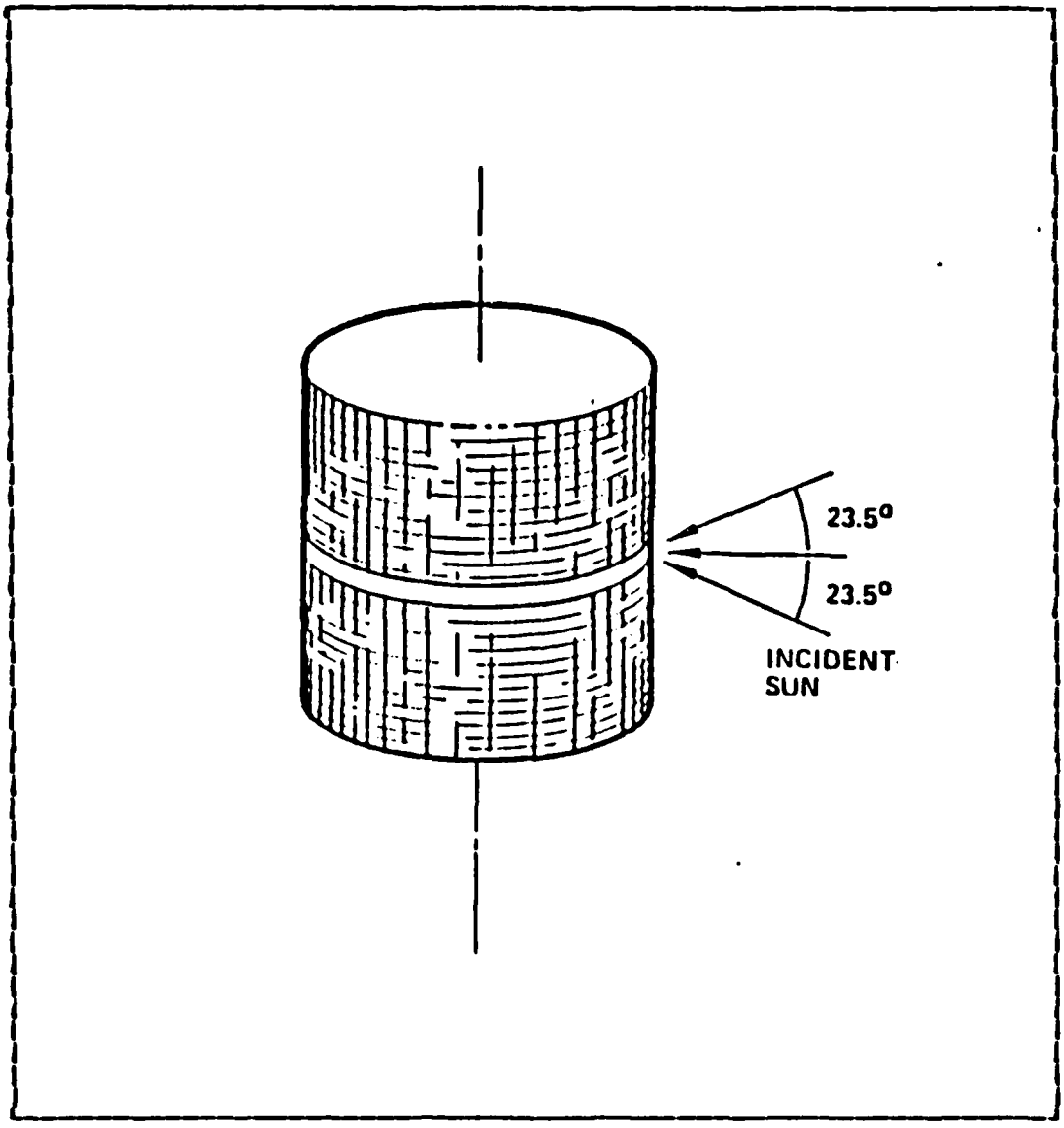

Figure 3.4 Cylindrical Panel Installation

degradation is shown is Figure 3.6 [Ref. 9:p. 1-7.13]. Damage is a result of charged particles creating defects in the n and p layers of the cell. The net result is shown in Figure 3.7. For any set of four sequential peaks, the maximums correspond to the autumnal and vernal equinox and the minimums correspond to summer and winter solstice when sun incidence is offset by 23.5 degrees.

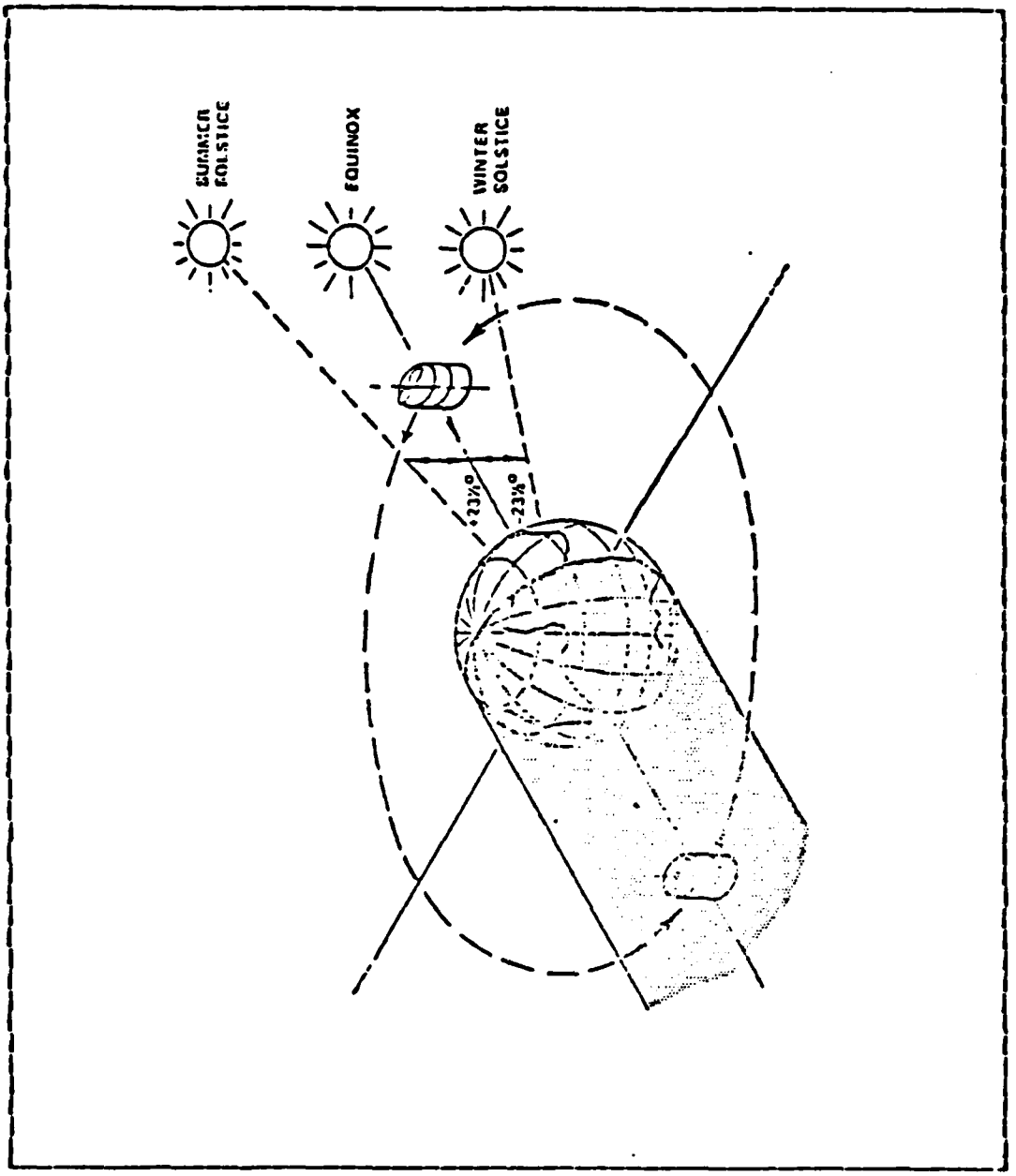

Figure 3.5 Solar Incident Angle

The satellite that is being proposed will have a diameter of 5.7 feet and a height of 10 feet. This gives a projected area of 57 square feet. At beginning-of-life (BOL) solar cells produce approximately 11 watts of power per square foot of area. Thus the 57 square feet will yield

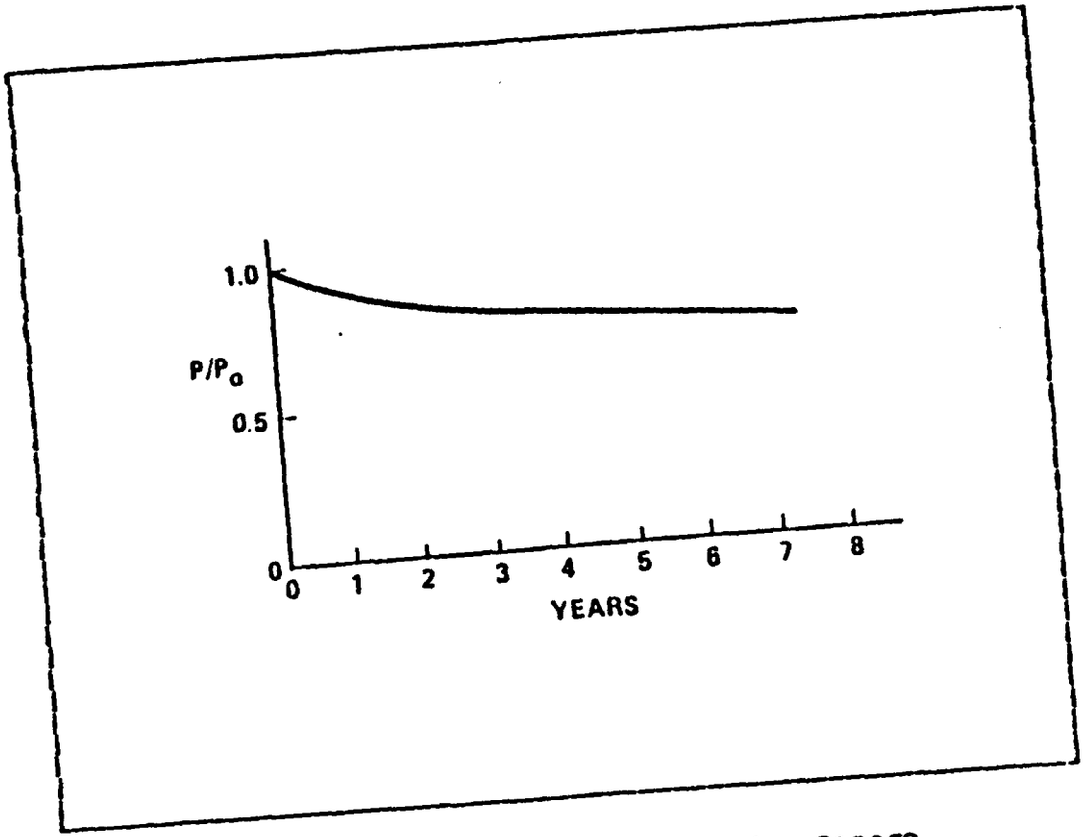

Figure 3.6 Solar Cell Radiation Damage

627 watts of power. This initial power level will decrease because of the factors mentioned previously. From Figure 3.6, after seven years on-station, the power level will have fallen to approximately 72 percent of the BOL value. This leaves 451 watts of available power. A second correction factor can be obtained from Figure 3.7. During any given year the lowest power output is during summer solstice. The highest power output is the immediately preceding vernal equinox. Using the time during the third to fourth years on the graph, the correction factor is

(3.27)

$$553/625 = .8848$$

The power that will be available at end-of-life during summer solstice will then be approximately 400 watts. The

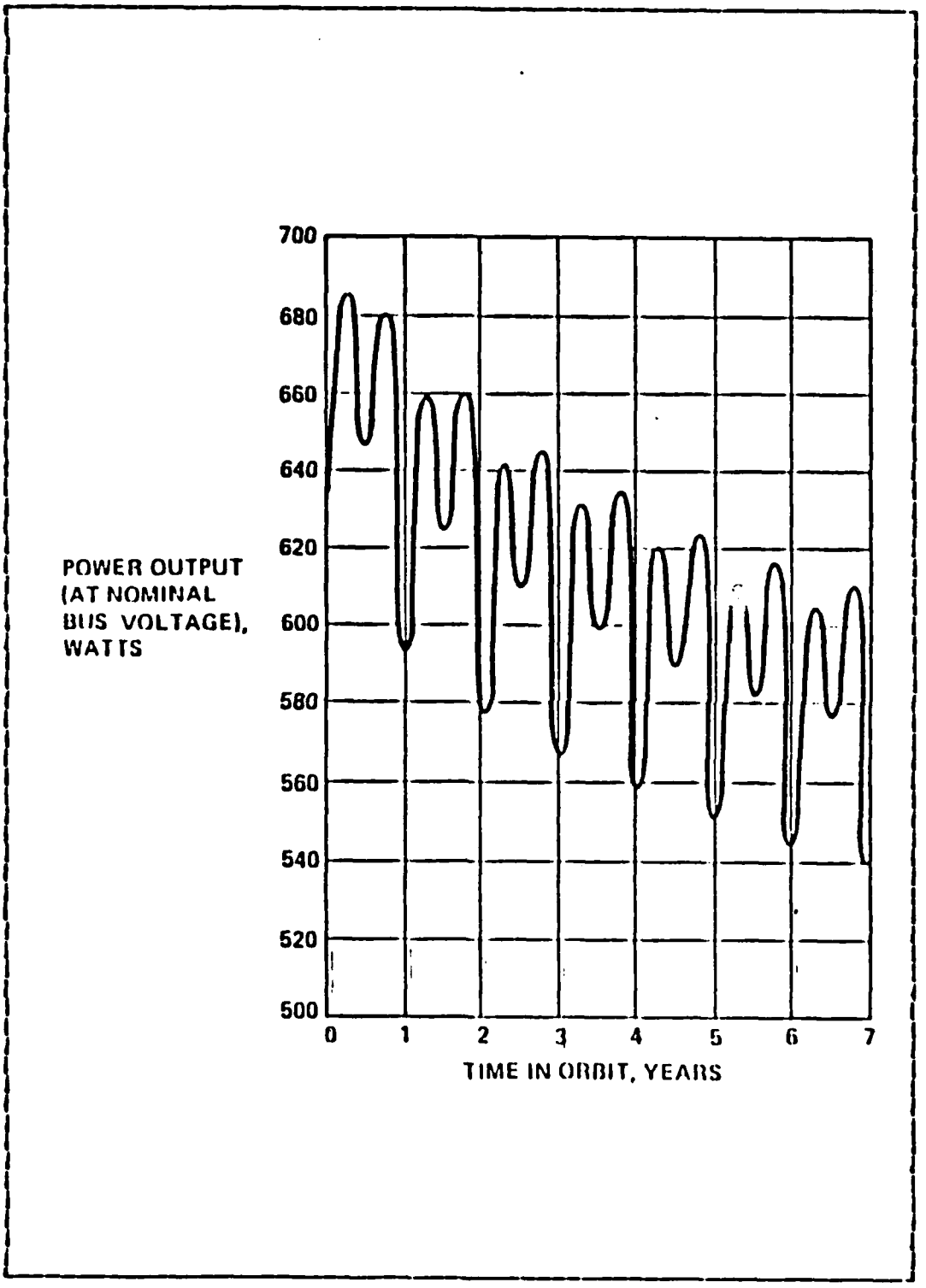

Figure 3.7 Panel Output VS Time

electrical power budget must be based on this EOL value. The power-to-mass ratio at EOL for solar cells is approximately 20 watts/kg for normal incidence [Ref. 10:p. 73]. This ratio must be decreased because the satellite does not have flat plate collectors. The amount of decrease will be the ratio of the area of a flat plate collector to the area of the illuminated half cylinder. The area of an equivalent flat collector is 57 square feet. The surface area of the half cylinder (A_c) is

$$A_c = (.5)(2\pi rh) \tag{3.28}$$

$$= (\pi)(5.7/2)(10) \tag{3.29}$$

$$= 89.5 \text{ ft}^2 \tag{3.30}$$

The power-to-mass ratio of the cylinder (P_c) is then

$$P_c = (20)(57/89.5) \tag{3.31}$$

$$= 12.73 \text{ watts/kg} \tag{3.32}$$

The mass of the solar cells (M_c) is then

$$M_c = 200/12.73 \tag{3.33}$$

$$= 15.7 \text{ kg} \tag{3.34}$$

This is the mass of only those cells that are receiving

sunlight. The total mass is twice as much. Converting kg to pounds will give a total weight of the solar cells as 69 pounds.

2. Battery Requirements

Batteries that are used in a weightless environment can not be of the "flooded" electrolyte type such as lead-acid cells. Rather, the electrolyte must be absorbed in the separator material to assure even distribution. The two primary types of batteries that meet this condition are the sealed silver-zinc and the nickel-cadmium.

Table II [Ref. 9:p. 1-7.17] shows the major characteristics of concern for both battery types. Nickel-cadmium batteries will be used because of their longer life expectancy and tolerance to overcharge allowing a simpler charge control circuit. The major disadvantage will be an increase in weight due to the lower energy density.

The satellite will be spending 50 percent of its time in the Earth's shadow during which the battery must supply the electrical power. During the time sunlight is available, the battery must be recharged. Since equal amounts of time are spent in light and shade, half of the solar panels must be dedicated to battery charging and the remaining half to satellite bus power. The time the satellite is in darkness (T_d) can be found from Equation 2.10 to be

$$T_d = .5T_c \tag{3.35}$$

$$= (\pi)(6692 \times 10^3)^{3/2}/\mathrm{SQRT}(3.99 \times 10^{14}) \tag{3.36}$$

$$T_d = 45.4 \text{ min} \tag{3.37}$$

TABLE II

BATTERY CHARACTERISTICS

TYPE	ENERGY DENSITY, W HR/LB	CYCLE LIFE RANGE	LIFE EXPECTANCY	THERMAL CONSIDERATIONS	CHARGING CONSIDERATIONS
AG-ZN	50 TO 60	20 TO 200	6 TO 12 MO	1) GOOD HIGH TEMP DISCHARGE PERFORMANCE 2) DEGRADED DISCHARGE PERFORMANCE AT LOW TEMP	1) CURRENT/VOLTAGE LIMIT 2) CONTROL OF OVERCHARGE IS CRITICAL
NI CD	10 TO 12	200 TO 10^4	3 TO 7 YR	1) GOOD DISCHARGE PERFORMANCE AT LOW/MODERATE TEMP 2) DEGRADED DISCHARGE PERFORMANCE AT HIGH TEMP	1) CURRENT LIMIT 2) OVERCHARGE AT MODERATE RATES NOT CRITICAL (SHOULD BE MINIMIZED FOR LIFE CONSIDERATIONS)

The satellite system will be drawing 200 watts of power during this time and the watt-hours required from the battery (P_b) will be

$$P_b = (200)(45.4/60) \tag{3.38}$$

$$= 151.3 \text{ watt-hours} \tag{3.39}$$

Figure 3.8 [Ref. 9:p. 1-7.21] shows that as the depth of discharge (DOD) decreases the lifetime of the battery increases. In order to have a long lifetime, a high capacity battery system is desirable but the penalty is additional weight. From Reference 10, the battery system on the Intelsat V can supply 34 amp-hours at 27 volts and has a mass of 32 kg [Ref. 10:p. 73]. This gives a battery energy density of 13 watts/pound which is slighty better than shown in Table II. To provide a low DOD but not require excessive weight, the battery system for the proposed satellite will be capable of supplying 1200 watt-hours. This gives a DOD of

$$DOD = 151.3/1200 \tag{3.40}$$

$$= 12.6 \text{ percent} \tag{3.41}$$

From Figure 3.8 this gives approximately 23,000 cycles for the battery. The time for one cycle is 90.8 minutes. There are 5,789 cycles completed in one year. Thus the battery has a lifetime of approximately four years and will weigh about 92 pounds.

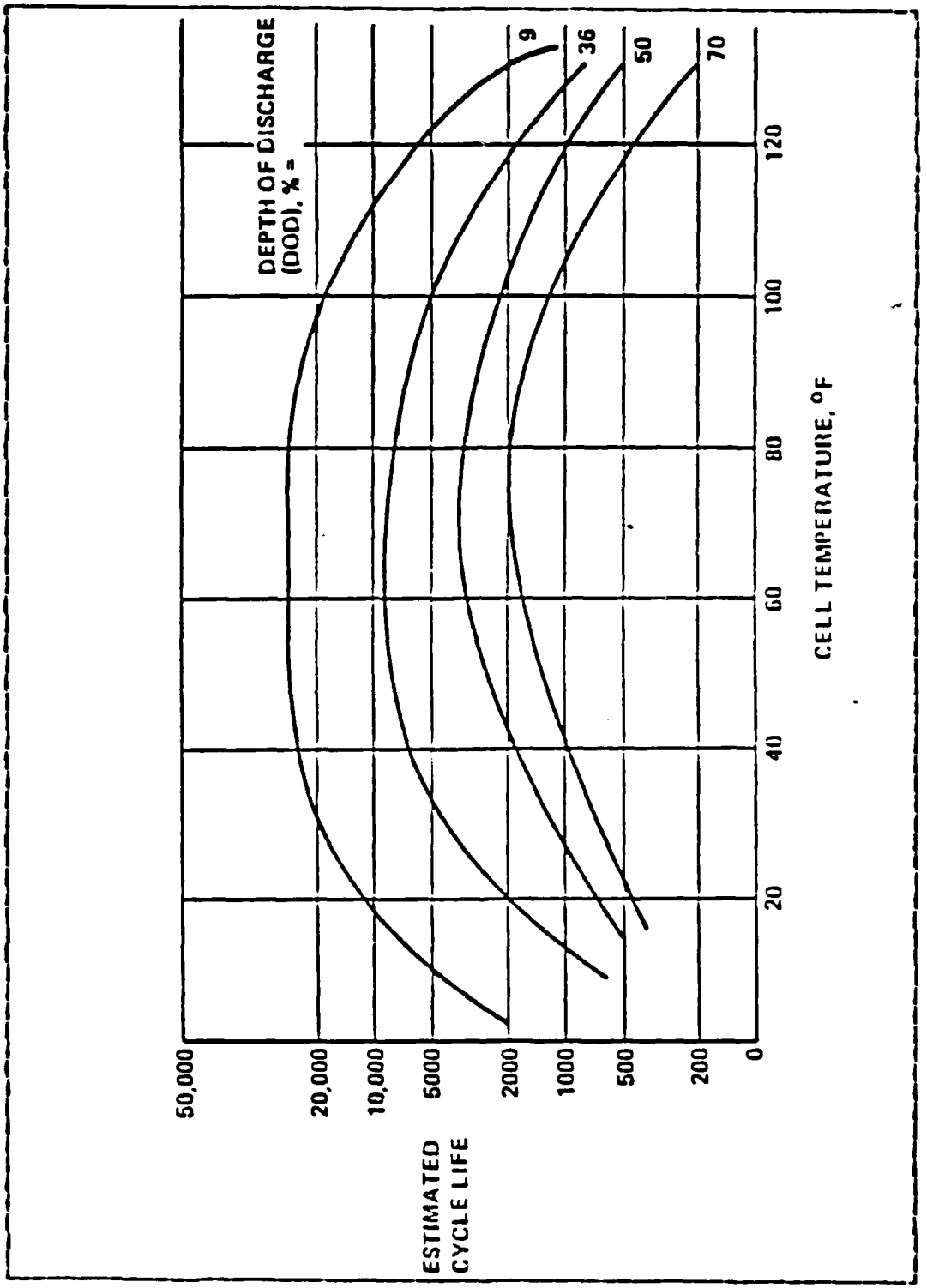

Figure 3.8 Nickel-Cadmium Battery Cycle Life

E. SYSTEM WEIGHT AND POWER BUDGET

The satellite has an on-orbit weight of 500 pounds. Subtracting 30 pounds for the antenna, 69 pounds for the solar cells and the battery weight of 92 pounds leaves 309 pounds for the remaining electronics, structure and control systems. Using the weight and power ratios in Reference 10 gives the results shown in Table III.

TABLE III
WEIGHT AND POWER BUDGET

System	Weight (lb)	Power (watts)
Antenna	30	-------
Solar Cells	69	-------
Battery	92	-------
Telemetry, Command	16	7.9
Attitude Control	43	9.6
Propulsion	24	1.0
Structure	86	-------
Electrical Integration	25	20.3
Signal Processing	115	161.2

Of the 161.2 watts available for signal processing, approximately 30 percent would be available for use to transmit data back to central Earth collection stations. The signal strength at the surface of the Earth can be calculated by

$$P_r = \frac{P_t (G_t G_r) \lambda^2}{(4\pi)^2 r^2} \qquad (3.42)$$

P_t is the transmitted power, G_t and G_r are the gains of the transmitting and receiving antennas and r is the distance between the satellite and Earth. Using the designed antenna as the transmitting antenna, the gain is 11.36 dB with reference to an isotropic radiator. An Earth based antenna does not have the same weight constraints and could be designed for a gain of 150. Using these values, the received signal power would be 0.63 microwatts.

F. STABILITY

The satellite is designed to spin about its longitudinal axis. If it were to tumble about its transverse diameter, it would be totally inoperative. An analysis of the moment of inertia about both axes is required to ensure proper placement of the internal components. From Reference 11 the moment of inertia for a hollow circular cylinder of length h about the longitudinal axis is

$$I_g = (m/2)(R_i^2+R_o^2) \tag{3.43}$$

R_i and R_o are the inner and outer radii and m is the mass of the cylinder. The moment of inertia about the transverse diameter is

$$I_t = m\left[\frac{R_i^2+R_o^2}{4} + \frac{h^2}{12}\right] \tag{3.44}$$

For stability, I_g must be greater than I_t. The longitudinal moment of inertia due to the solar cells with $R_i=R_o$ yields 560.4 ft²-lb. The corresponding transverse moment of inertia is 655.2 ft²-lb. In order to increase I_g more than I_t, weight must be distributed in a disk-like manner at the center of the satellite. The weight of the antenna, solar cells and structure can not be centralized. The remaining weight is 315 pounds. This weight with R_i equal to zero adds 1279.3 ft²-lb in the longitudinal direction for a total

of 1839.7 ft^2-lb. It is now necessary to determine the maximum height (d) of the disk. The total transverse moment of inertia must be less than 1839.7 ft^2-lb. That is

$$1839.7 > (315/2)[.5(5.7/2)^2+d^2/6]+855.2 \quad (3.45)$$

$$6.25-4.06 > d^2/6 \quad (3.46)$$

$$d < 3.6 \text{ feet} \quad (3.47)$$

IV. DESCRIPTION OF RESEARCH

A. DESIGN OVERVIEW

The earthquake monitoring system is installed three miles east of San Juan Batista, Ca., and seven miles south of Hollister. It is located in the Hollister Hills State Vehicular Recreation Area (Upper Ranch) south of the MX track (see Figures 4.1 and 4.2). The site was chosen because it is both historically and recently an active earthquake area and is far enough from industrial areas to minimize manmade noise signals yet near possible earthquake sources to generate electromagnetic energy. Exact location is 1000 feet from the San Andreas fault at 121° 23.5' W and 36° 45.5' N.

Two frequencies (38.45 MHz and 150.75 MHz) are being monitored. These frequencies, each with a 50 KHz bandwidth, have been assigned to this project by the Army Frequency Coordinator for the Western United States for a renewable one year period. The antenna complex consists of two 20 foot towers and mounted antennas as shown in Appendix D. Each tower has five mounted antennas. Eight Yagi antennas sense horizontal and vertical polarization at each frequency both up and down the fault. Additionally, an omni antenna at each frequency is vertically mounted.

Each antenna signal is individually cabled to a modular AM receiver. Output from the receiver is sent to an interface amplifier where it is joined with a system timing signal. The composite signal is then sent to a chart recorder and permanently traced onto pressure sensitive paper. Figure 4.3 shows a block diagram for each channel with a single timer signal being common to all ten channels. All components are powered by 12 V DC. Collected data will be correlated to earthquake data provided by the Geological Survey Office, Menlo Park, Ca.

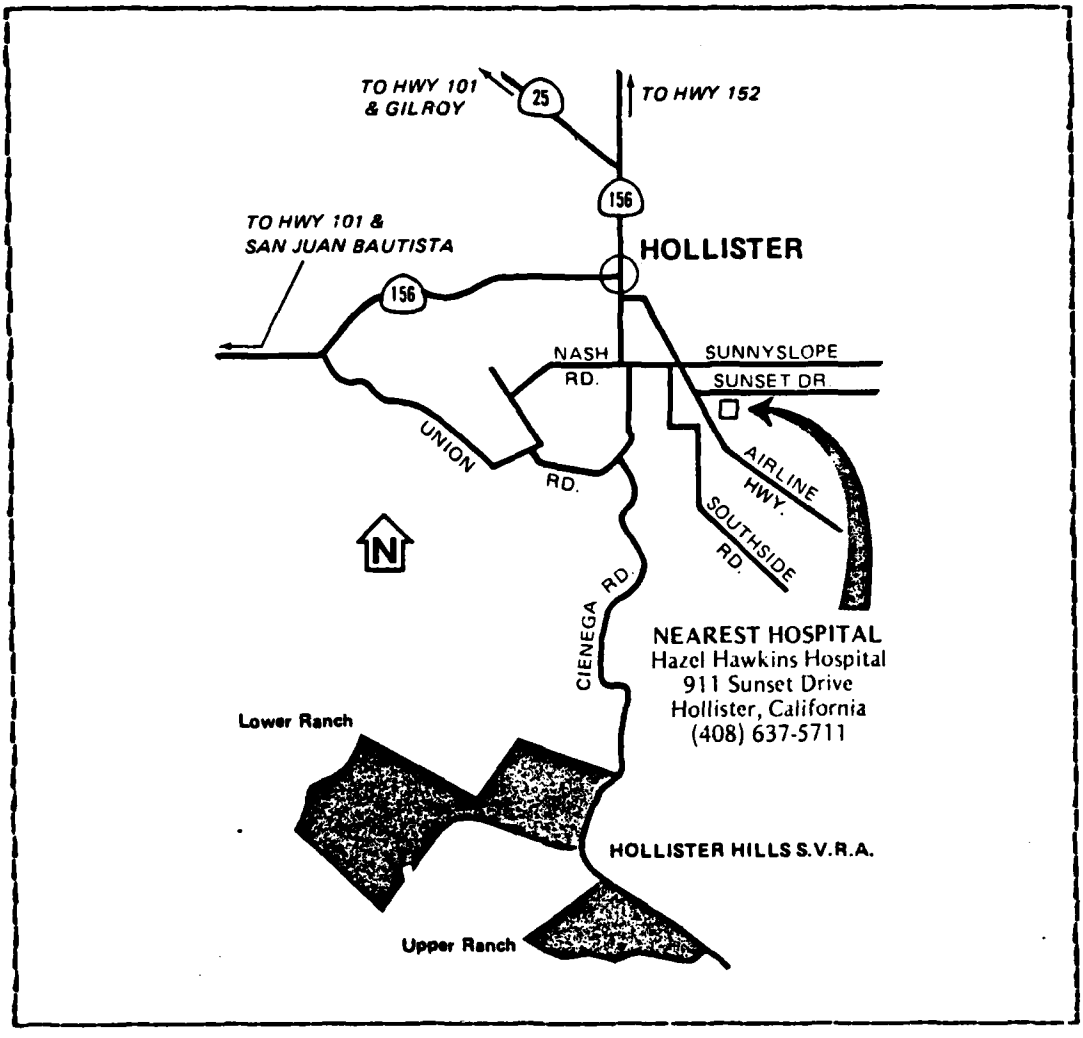

Figure 4.1 Site Location

B. SYSTEM COMPONENTS

1. Receivers

The antenna signal is coupled into the RF amplifier by a 50 ohm RCA jack. The oscillator frequency is determined by the crystal Y1. For 38.45 MHz, the crystal frequency is 49.15 MHz and for 150.75 MHz the crystal frequency is 46.68333 MHz. Figure 4.4 shows the schematic diagram for the 150.75 MHz receiver. The 38.75 MHz receiver does not have the Q4 multiplier circuit.

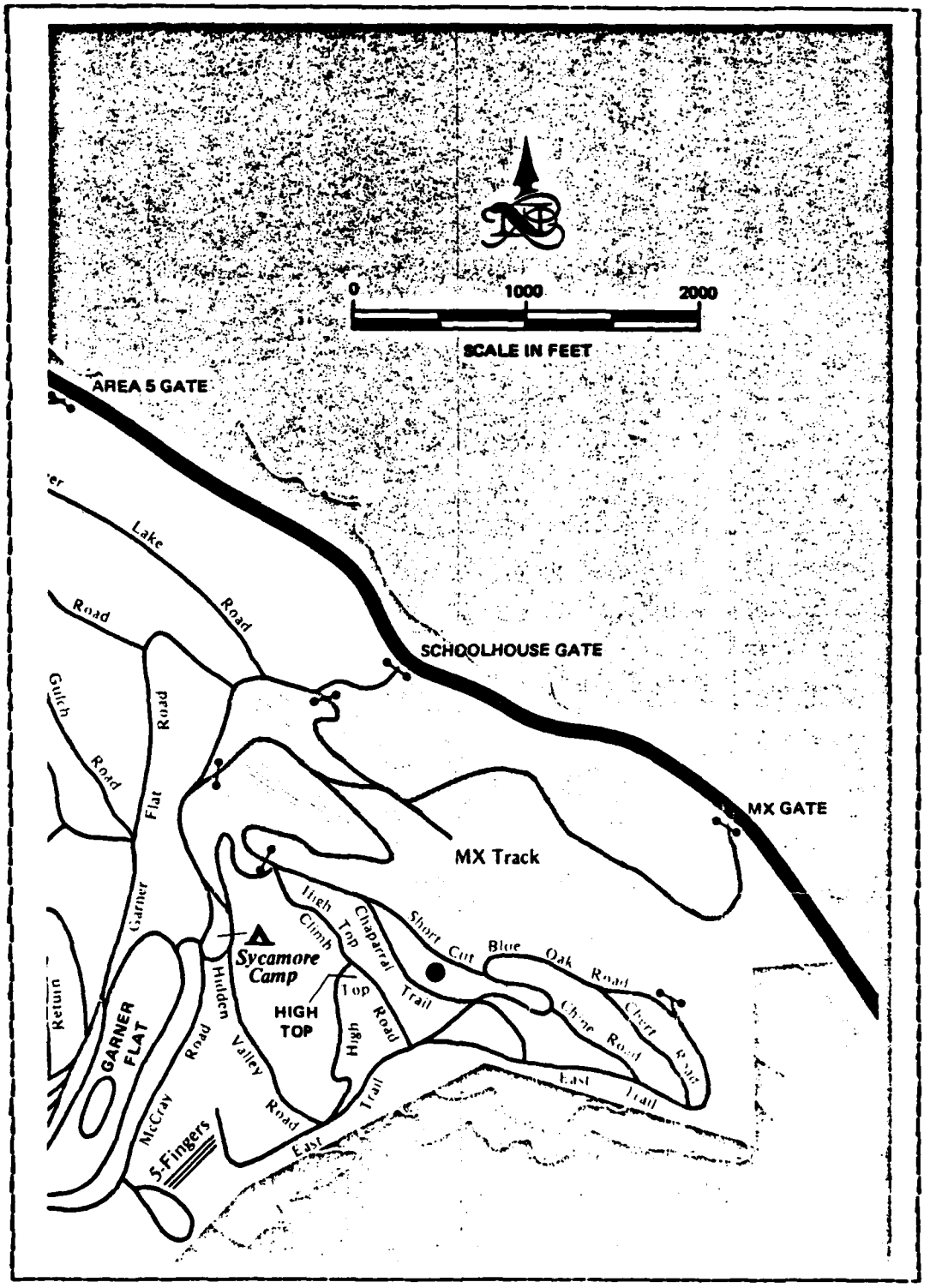

Figure 4.2 Site Location

The 10.7 MHz IF signal is sent to the IF-20 IF/Audio assembly. The signal is mixed with the 10.245 MHz oscillator frequency and down-converted to 455 KHz. This signal is then amplified and detected. The "S" meter output from an integral log detector is used as the input to the interface amplifier. Figure 4.5 is a schematic diagram for the IF/detector circuit. Appendix B contains measured receiver sensitivity curves.

2. Timer

In order to determine the time of data reception, the timer generates a voltage signal every 15 minutes, hourly and every 24 hours. The duration of this signal was modified from the original design to new values of 14 seconds for the 15 minute pulse, 42 seconds for the hourly pulse and 98 seconds for the 24 hour pulse. Accurate time is required to allow comparison with earthquake data. A 21 stage counter timer (RCA CD4045A) is crystal controlled and establishes a one second time reference for the entire system. Synchronous down counters (RCA CD40103B) then use this reference to generate signals at the appropriate times. The reset button is used to initialize or reset the zero time mark. A clock-running LED is used as a visual indication of proper operation and a pen-mark LED lights for each occurance of a time pulse and stays lit for its duration. The time pulse shows on the chart paper as a momentary increase in signal level and is above the local average recorded signal strength. Appendix C contains examples. Figure 4.6 is the schematic diagram.

3. Interface Amplifier

The "S" meter output from the receiver and the time pulse from the timer are integrated into one signal in the interface amplifier. This is accomplished by using operational amplifiers (LM 148/348). On Figure 4.7, R3 is used as a zero adjust to establish a zero-signal reference voltage. R10 adjusts the current to the chart recorders so

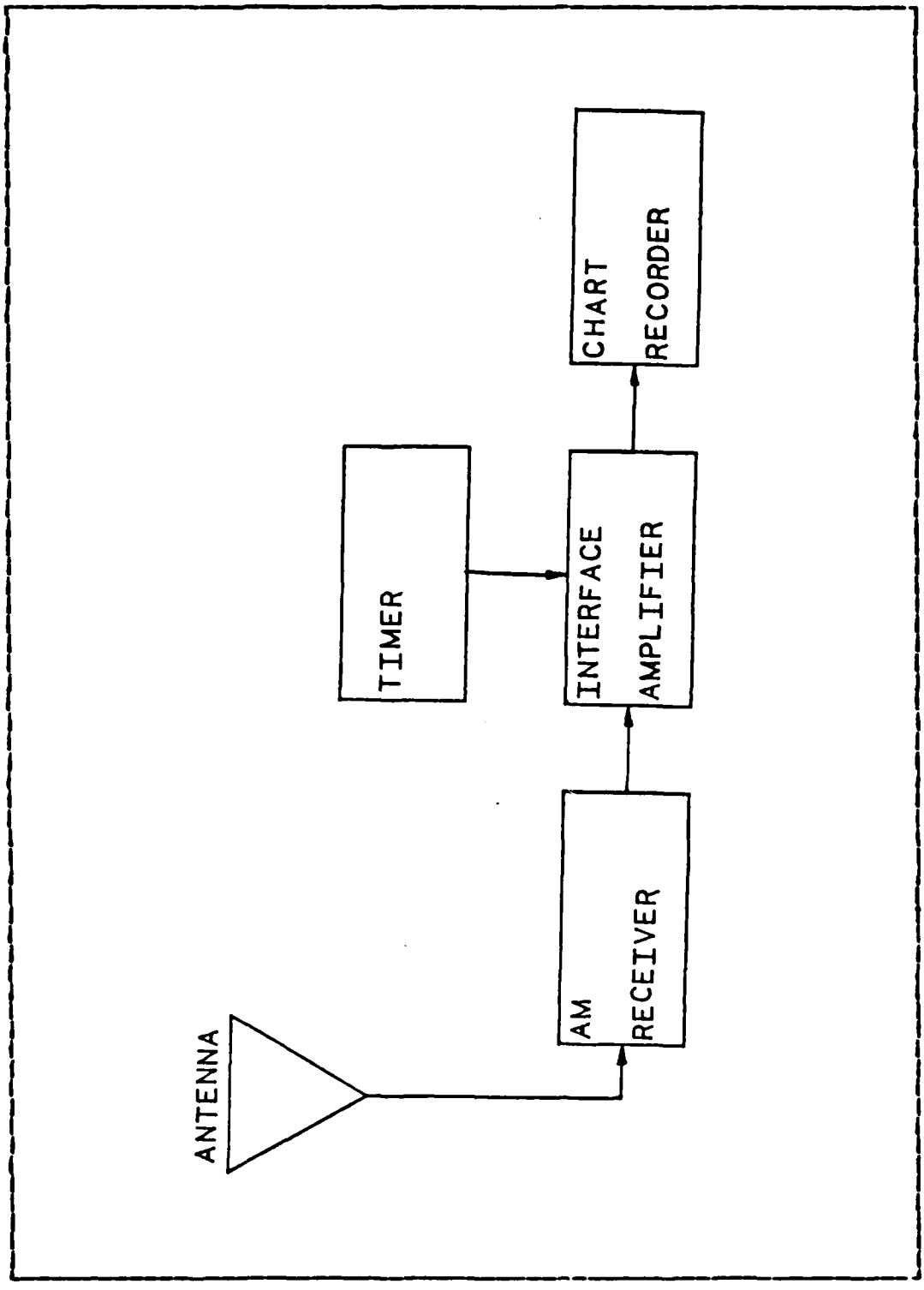

Figure 4.3 Monitoring System Block Diagram

the meter stylus can be set to its zero-signal position. R5 is then adjusted for full scale meter deflection at the desired RF signal strength and acts as a gain control.

4. Chart Recorders

The Rustrak recorder stylus is gear driven and strikes the pressure sensitive paper at regular intervals to produce an apparently continuous line. The stylus' position depends upon the current level through the meter. The paper speed is determined by interchangeable gear trains. Two styles of recorders are used and both are geared to allow one roll of paper to last two weeks. The main functional difference between the styles is the amount of current required for full scale deflection.

5. Battery Backup

Figure 4.8 shows the power supply block diagram. When 60 HZ, 115 volt power is available, the 12 volt power supply is used to provide system power. The relay contacts are held open by the 60 HZ power and the battery chargers maintain full charge on both batteries. The five diodes in series (for both positive and negative supplies) are reversed biased with no current flow. In the event AC power is lost, the relay contacts close and power is supplied by the batteries through the three parallel diodes. Three diodes in parallel were used for current handling and reliability reasons. When AC power is regained, the system returns to its original condition.

It was important to maintain power to the timer without interruption or the time sequence became scrambled. This is accomplished by the five series diodes for the time interval between losing AC power and the relay contacts closing. The parallel diodes drop the battery voltage by approximately 0.6 volts. This was necessary because the fully charged batteries produce 12.6 volts for several days. While not critical to the electronics portion of the system, the chart recorder paper drive motors are DC powered and the

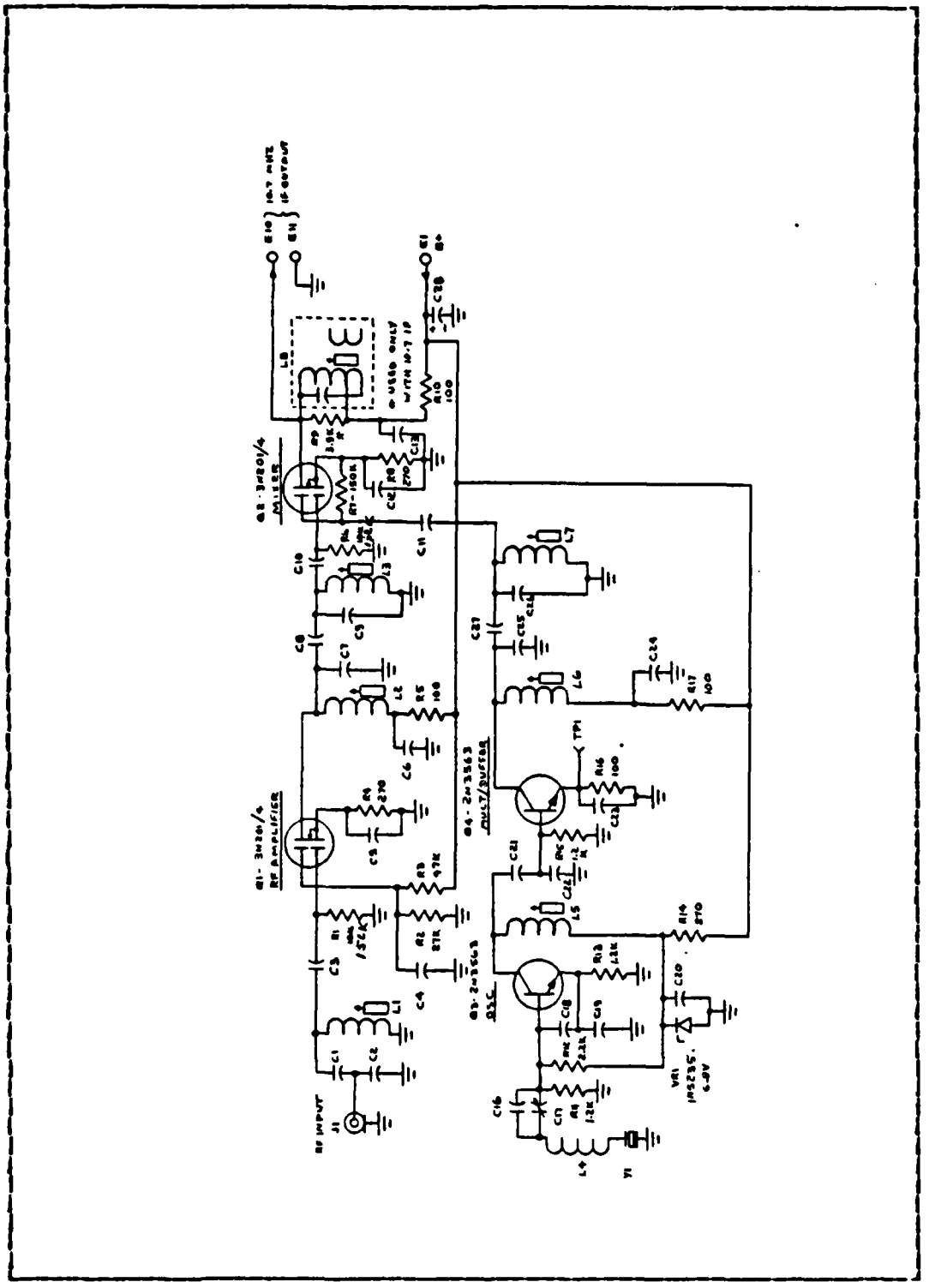

Figure 4.4 150.75 MHz VHF Converter

resultant increase in speed would result in running out of paper before the designed two weeks.

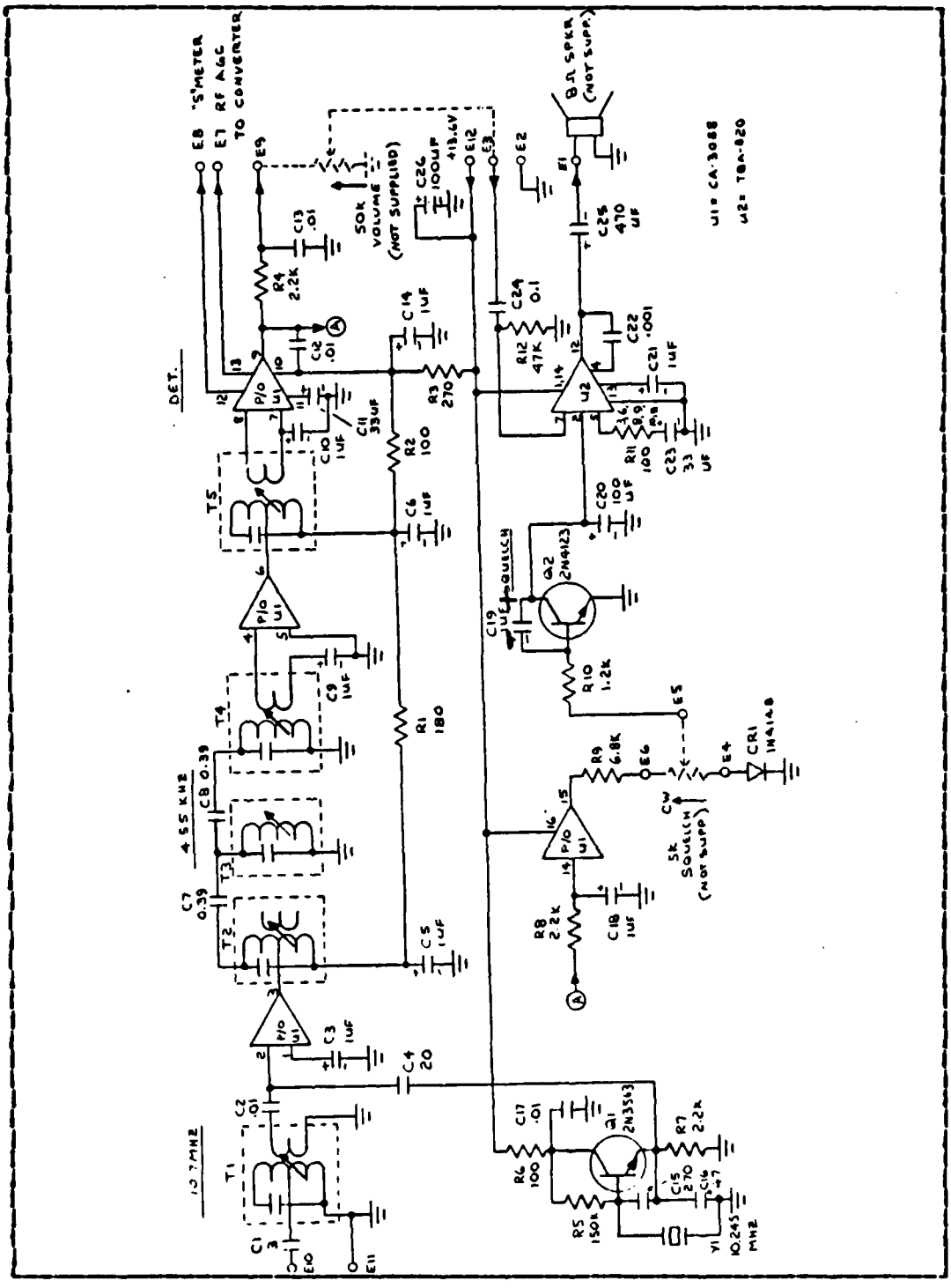

Figure 4.5 IF-20 IF/Audio Assembly

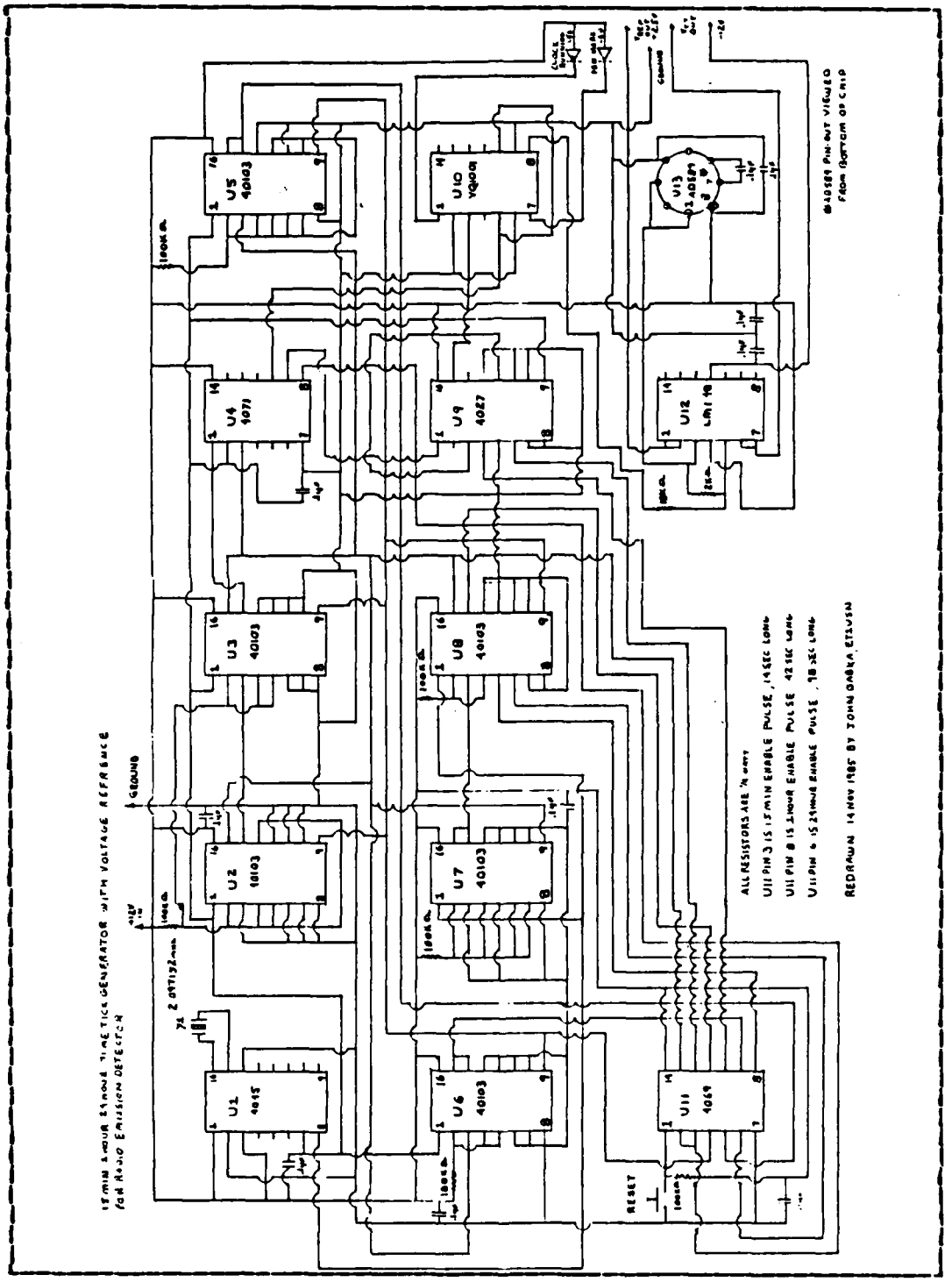

Figure 4.6 Timer and Reference Generator

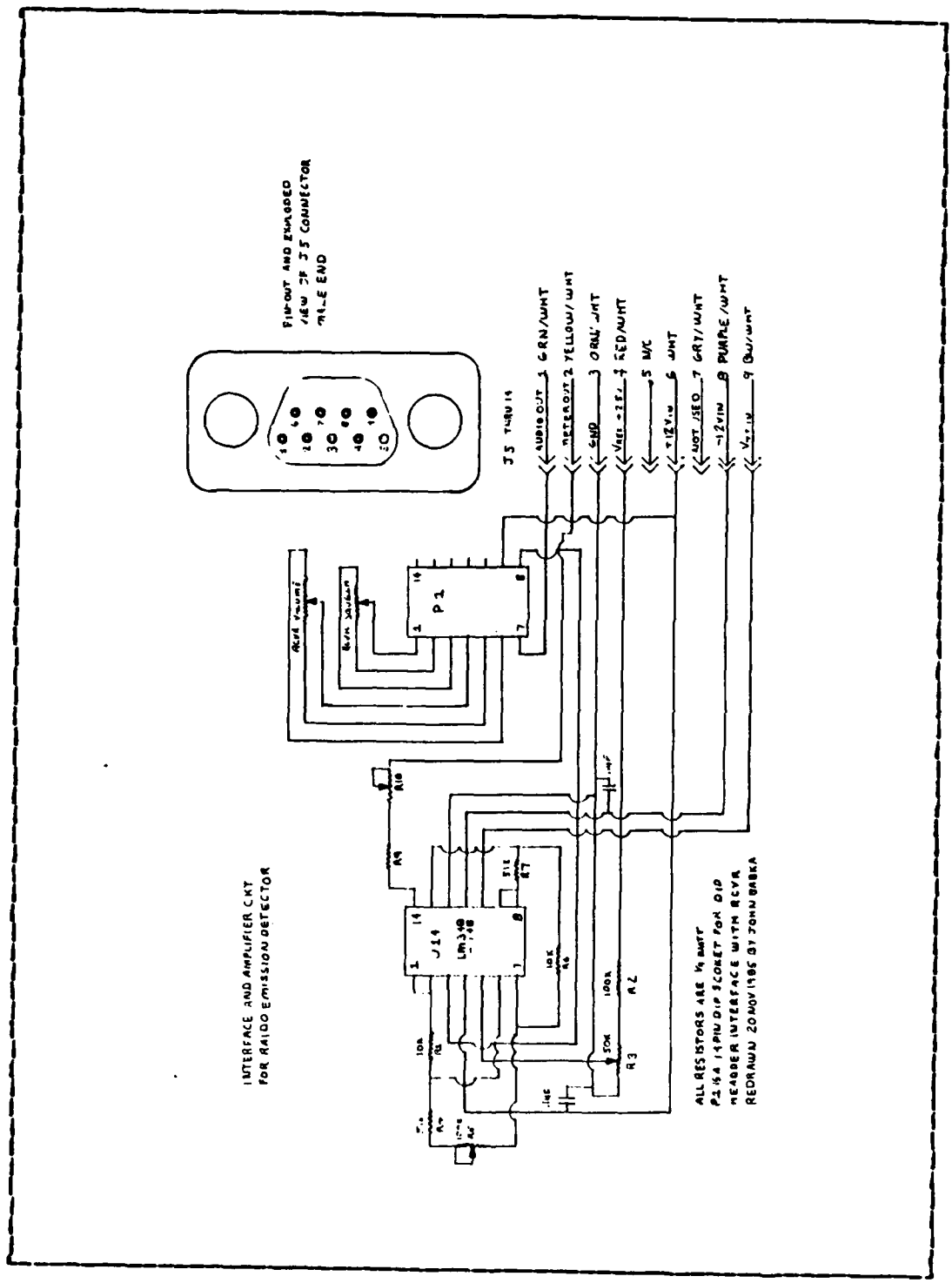

Figure 4.7 Interface Amplifier

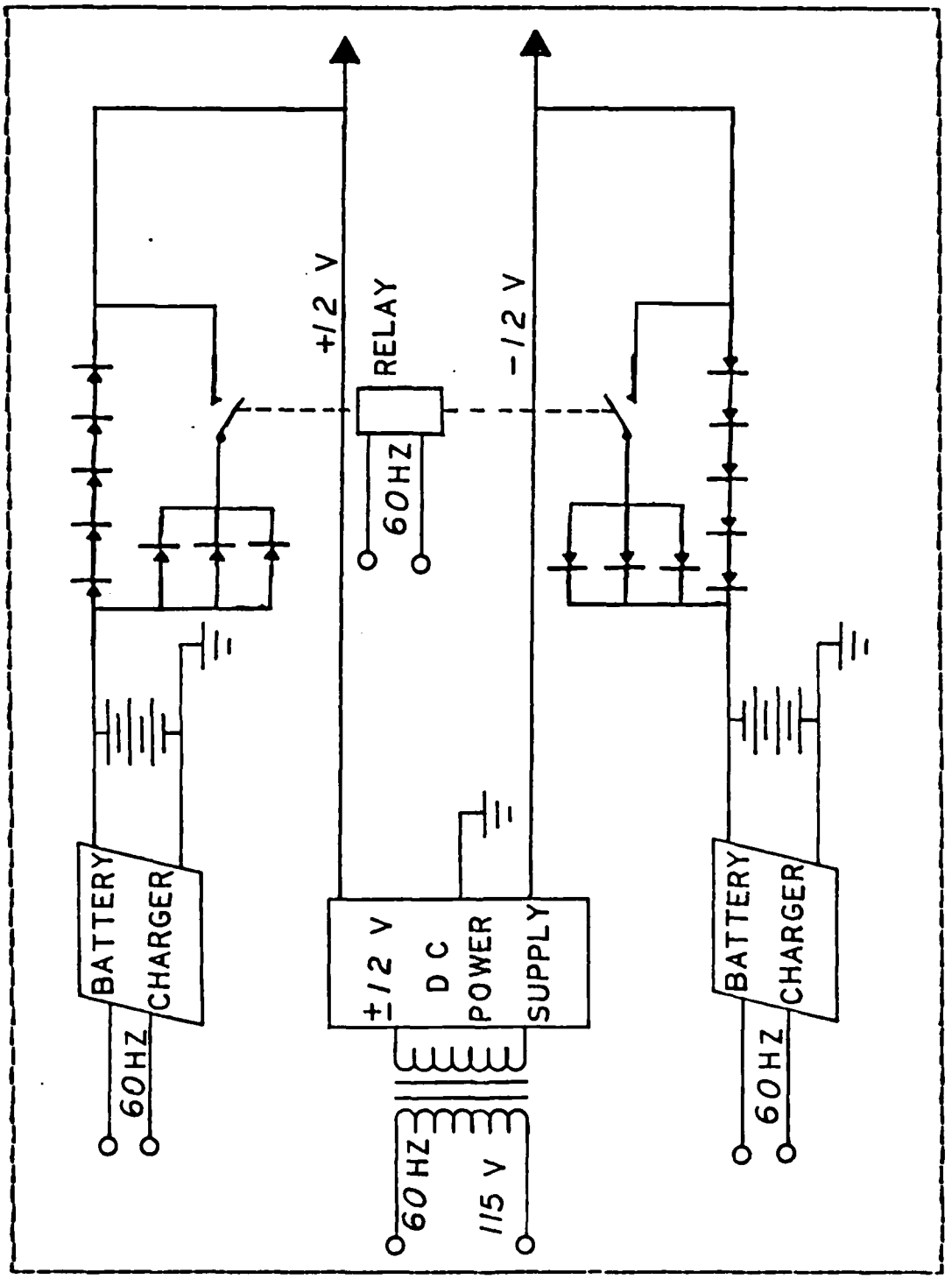

Figure 4.8 Battery Backup System

V. RESULTS AND CONCLUSIONS

A. RESULTS

The system installation was completed and began operation on November 8, 1985. The first set of strip chart recordings cover the time period of 8-22 November, 1985. Appendix C contains samples from channel seven which is at 150.75 MHz, vertically polarized, and looking toward the southeast. During the timeframe shown, three small earthquakes occured. The first was a magnitude 2.3 at 2044 on November 11, the second a magnitude 2.9 at 1411 on November 12 and the third a magnitude 2.04 at 0602 on November 13. No other channels recorded any signals during the same time period. The magnitude 2.3 was 17 miles from the antenna site with the other two being closer. All three were in a southeast direction from the antennas. Channel ten (38.45 MHz, omni) recorded two groups of signals with the first occuring during the three days preceding the quakes. The second group was two days after the quakes.

B. CONCLUSIONS

While no firm conclusions can be reached from such a limited set of chart recordings, the electromagnetic activity on channels seven and ten lend encouragement to the theory of earthquake generated RF energy. Additional recordings are required to confirm this theory or show just a random coincidence on the first attempt at data collection.

In order to show a connection, recordings should be continued for at least a year. Not only the simultaneous occurence but also those where a quake occured without recorded RF energy (and vice versa) would give valuable information concerning reliability and false alarm rate. Any relationship between the recorded signal level and the

magnitude of the quake or depth and linear distance of the epicenter from the antennas should also be investigated. The present equipment will provide an initial level of confidence on which to base a future decision of whether or not to continue the research. If sufficient evidence does exist to justify further time and monies, then more sofisticated and sensitive equipment will be required to detail any further relationships. The ideal system would include automated data collection similar to those currently in use by the Geological Survey Office. When sufficiently understood, the possibility of transferring the monitoring to a space-based sensor could finally be investigated with the advantages mentioned earlier.

APPENDIX A
CHANNEL CONNECTIONS

TABLE IV
CHANNEL CONNECTIONS

Channel	Frequency (MHz)	Polarization	Direction
1	150.75	V	NW
2	38.45	H	SE
3	150.75	OMNI	--
4	38.45	H	NW
5	150.75	H	SE
6	38.45	V	SE
7	150.75	V	SE
8	38.45	V	NW
9	150.75	V	NW
10	38.45	OMNI	--

V = Vertical
H = Horizontal
SE = South East
NW = North West

APPENDIX B
RECEIVER SENSITIVITY CURVES

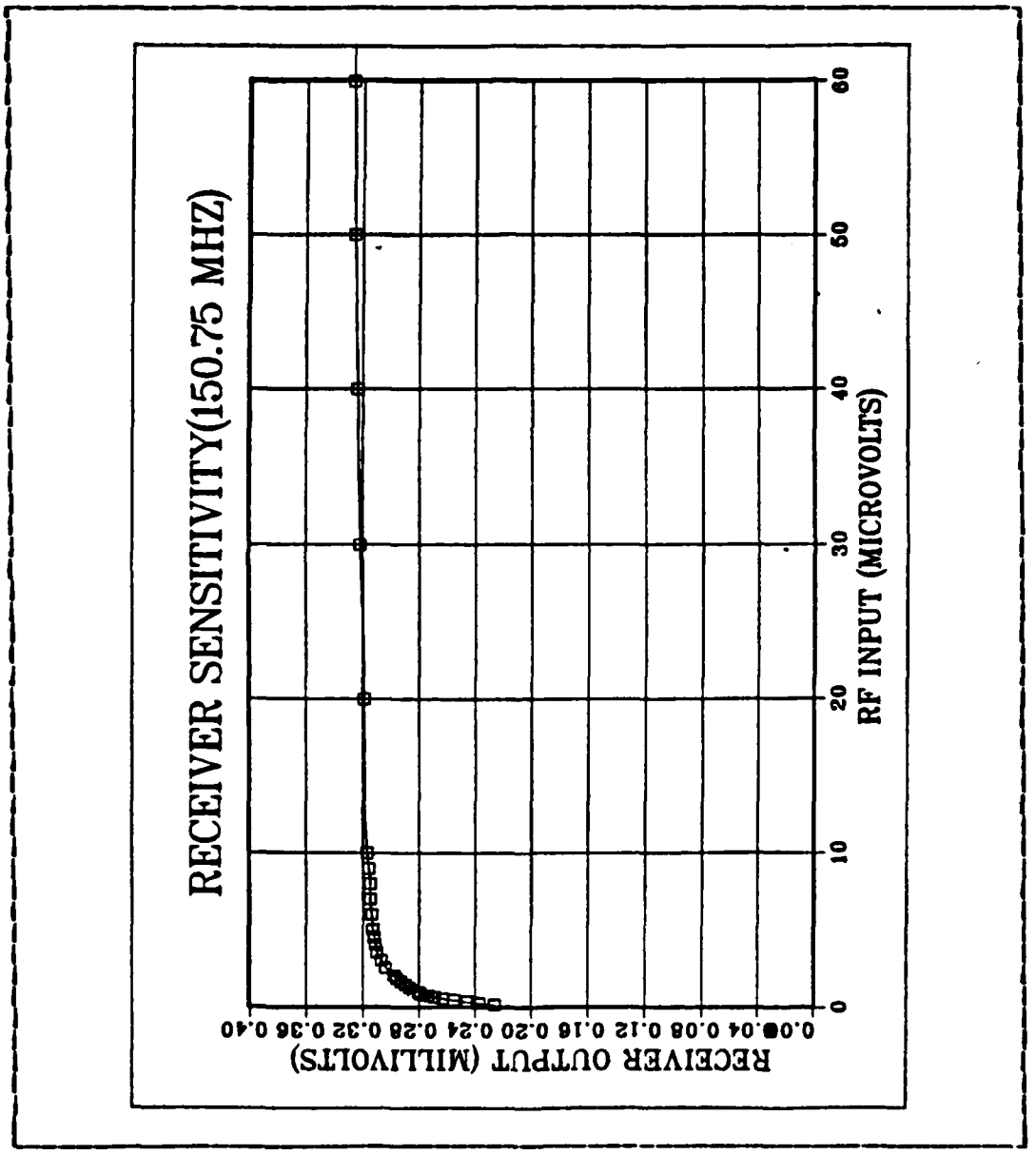

Figure B.1 150.75 MHz Response

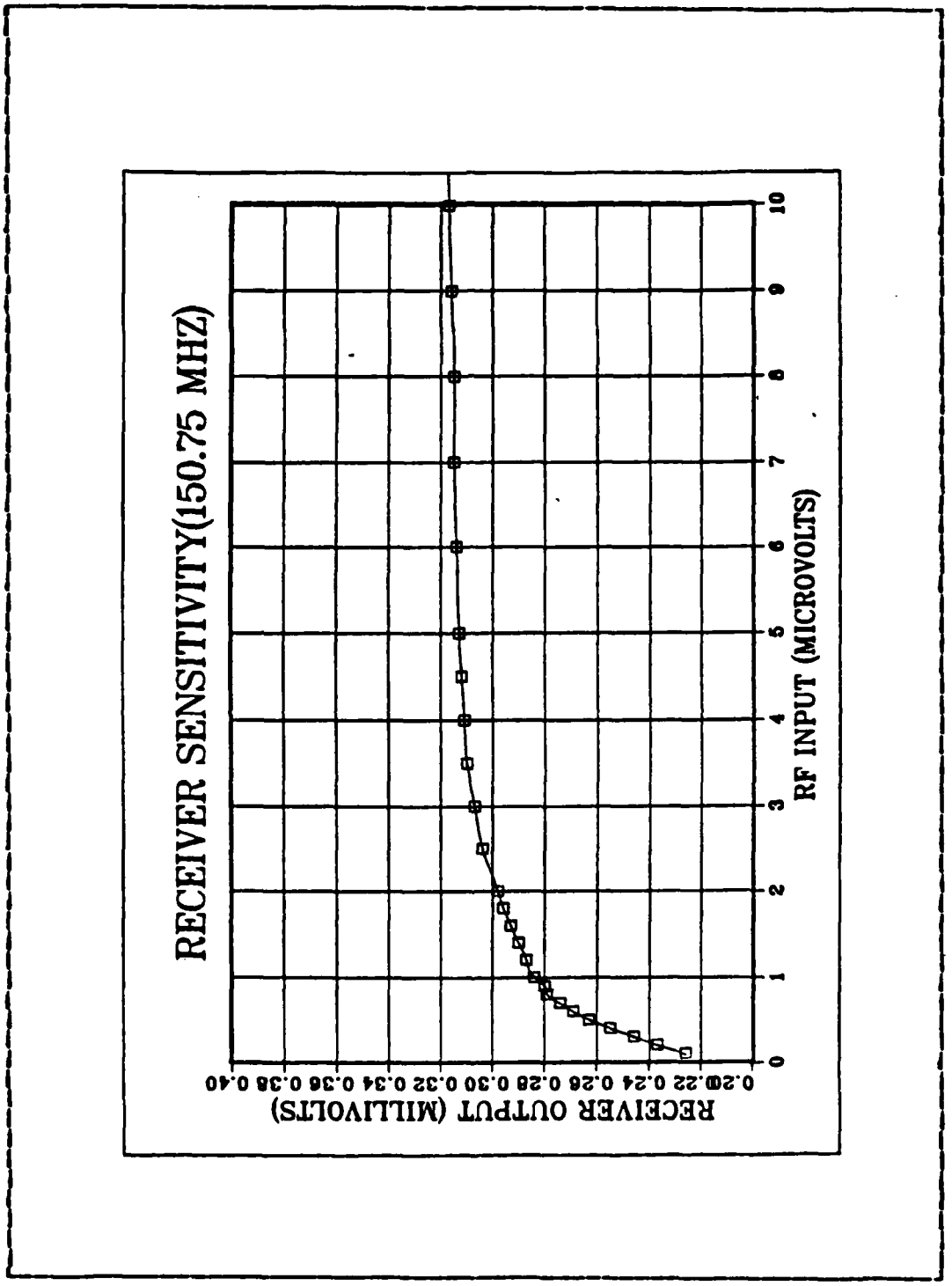

Figure B.2 150.75 MHz Response

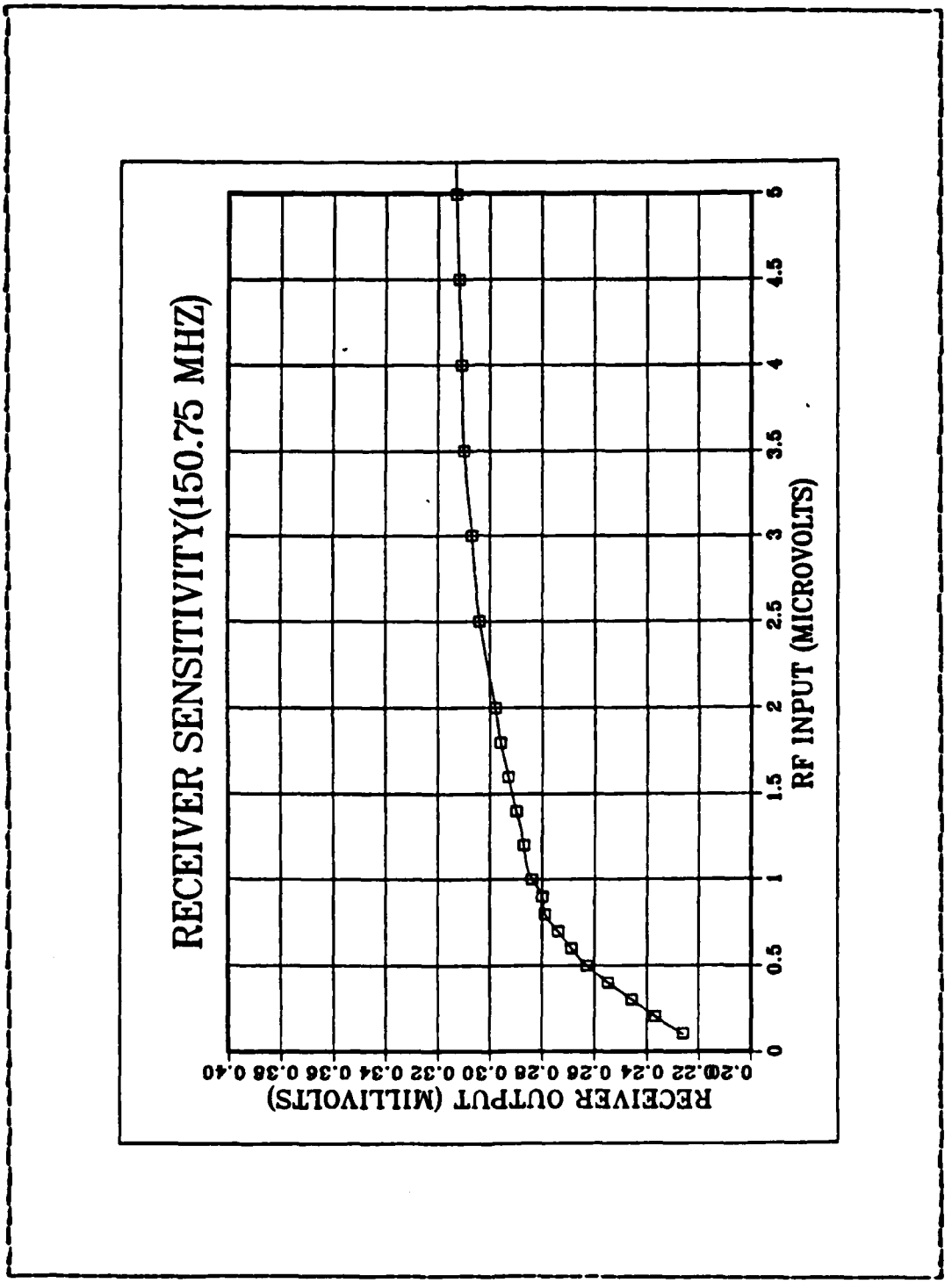

Figure B.3 150.75 MHz Response

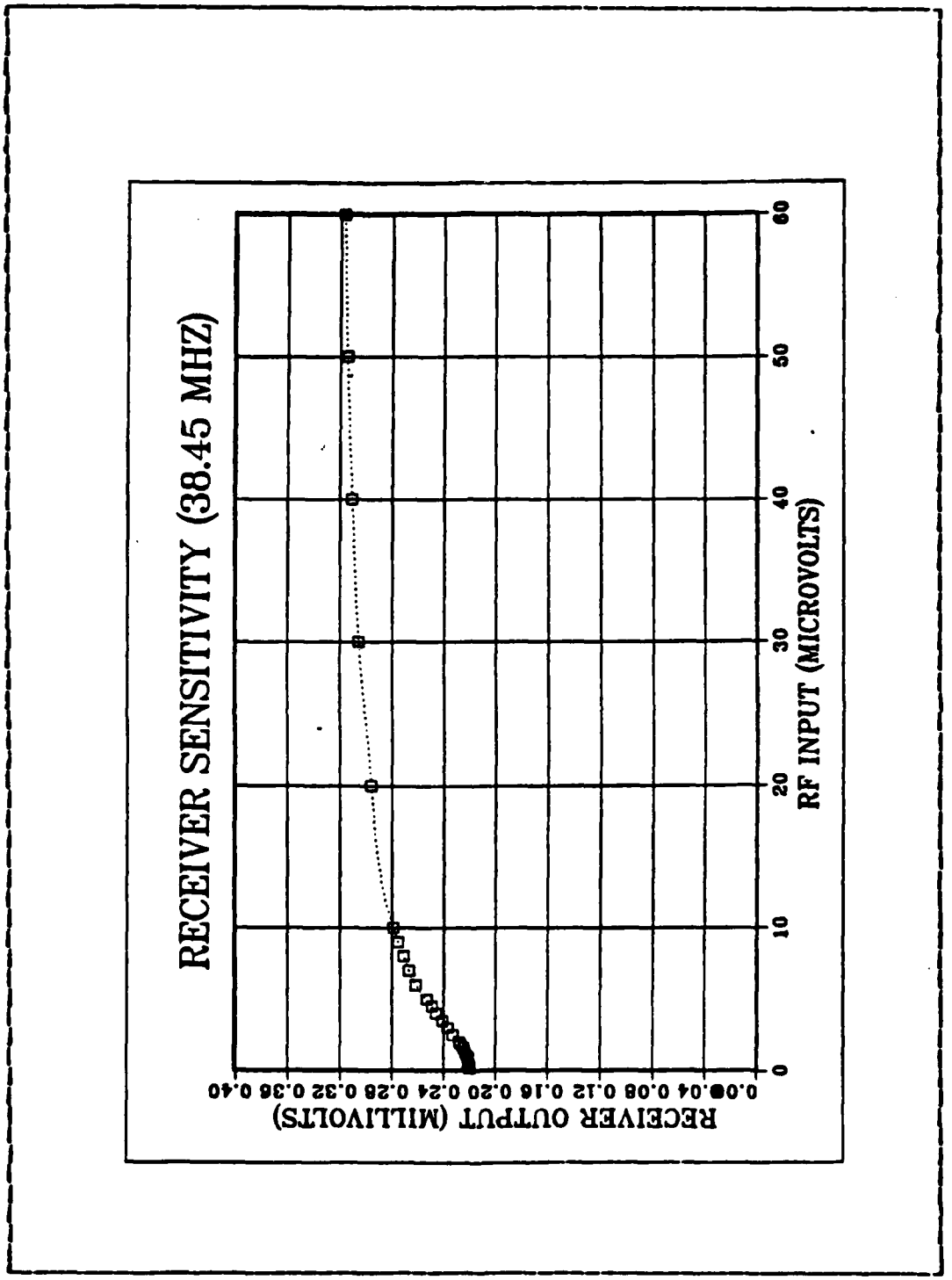

Figure B.4 38.45 MHz Response

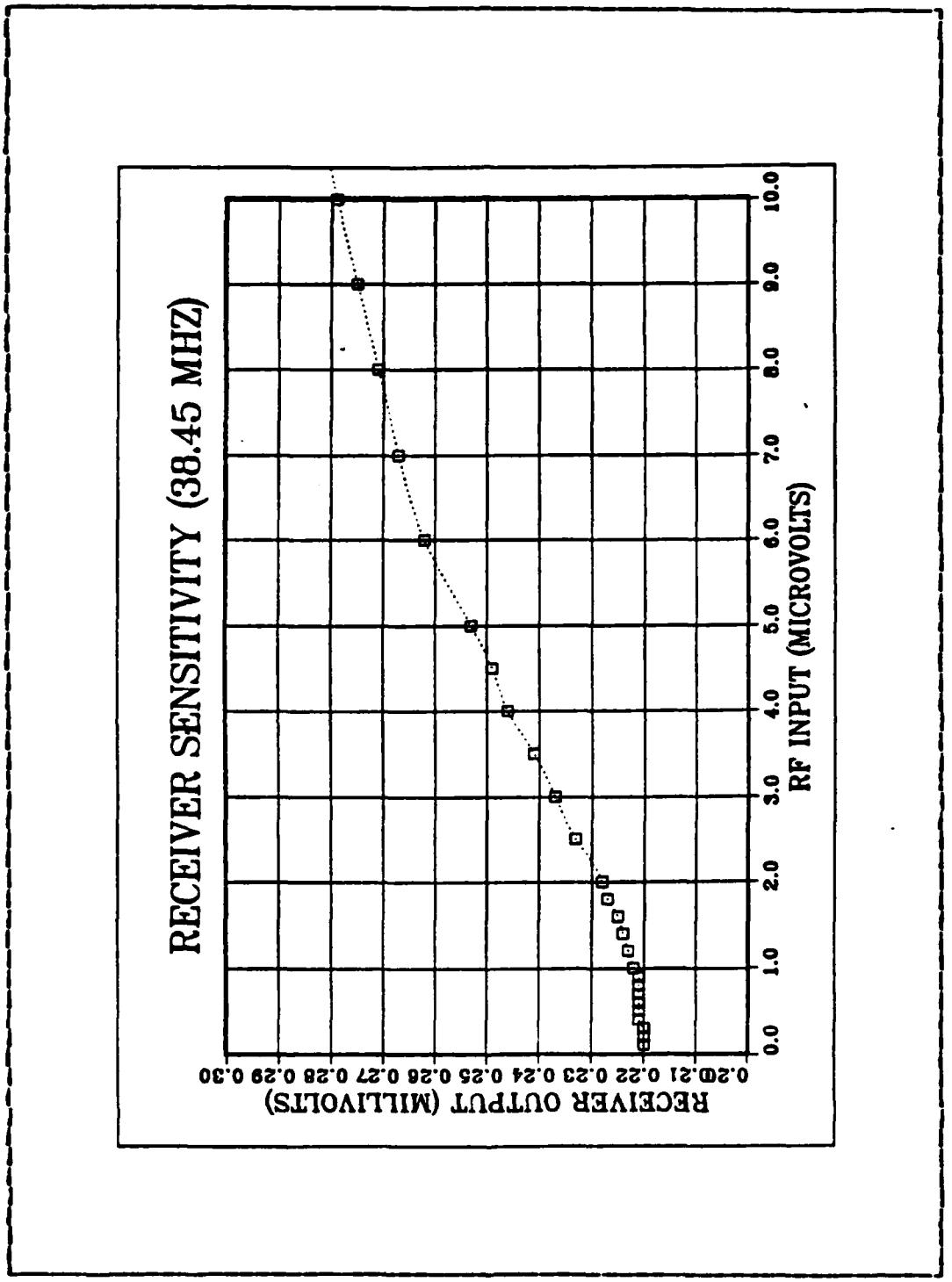

Figure B.5 38.45 MHz Response

APPENDIX C
CHART PAPER RECORDINGS

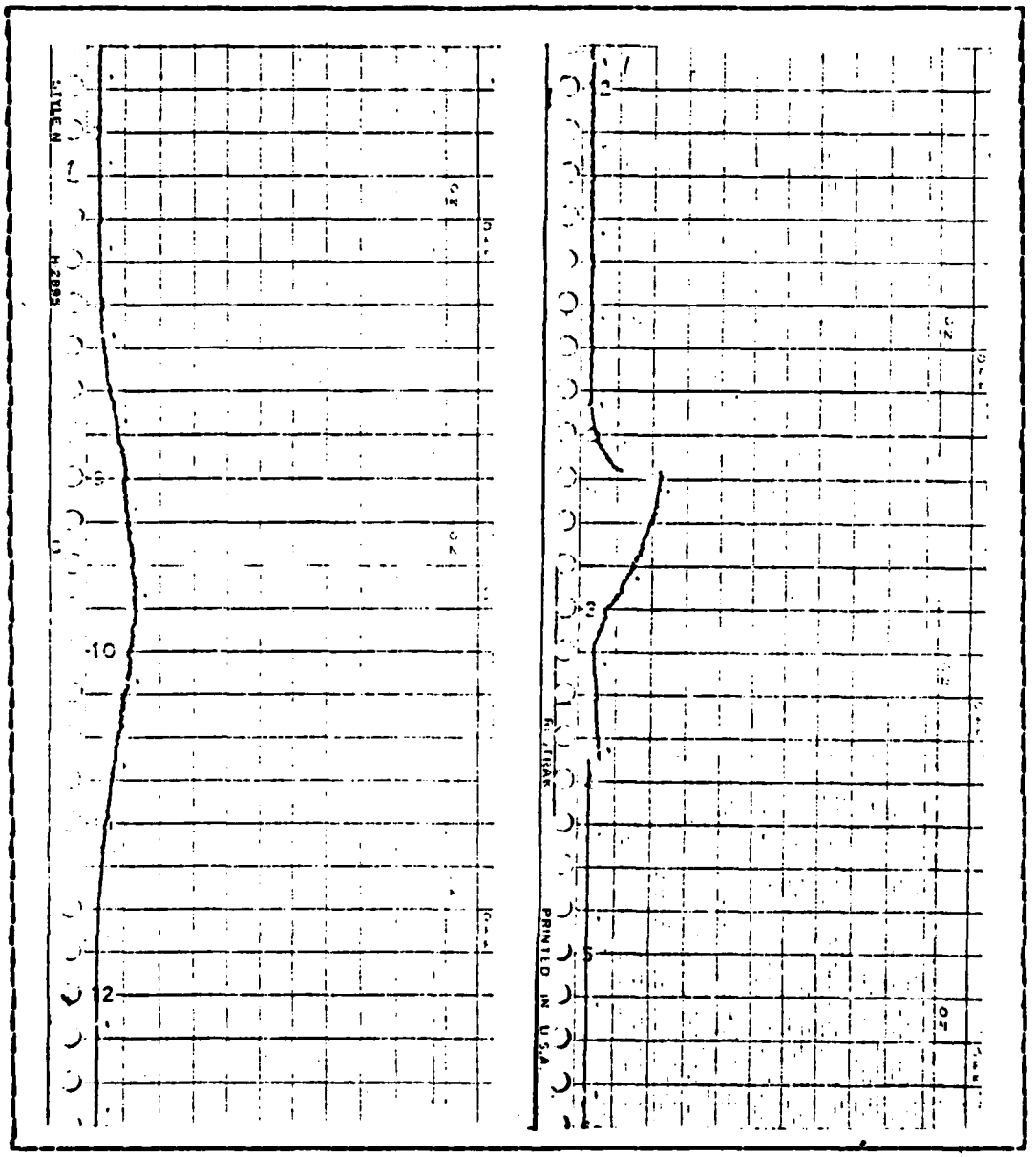

Figure C.1 Channel 7 Recordings

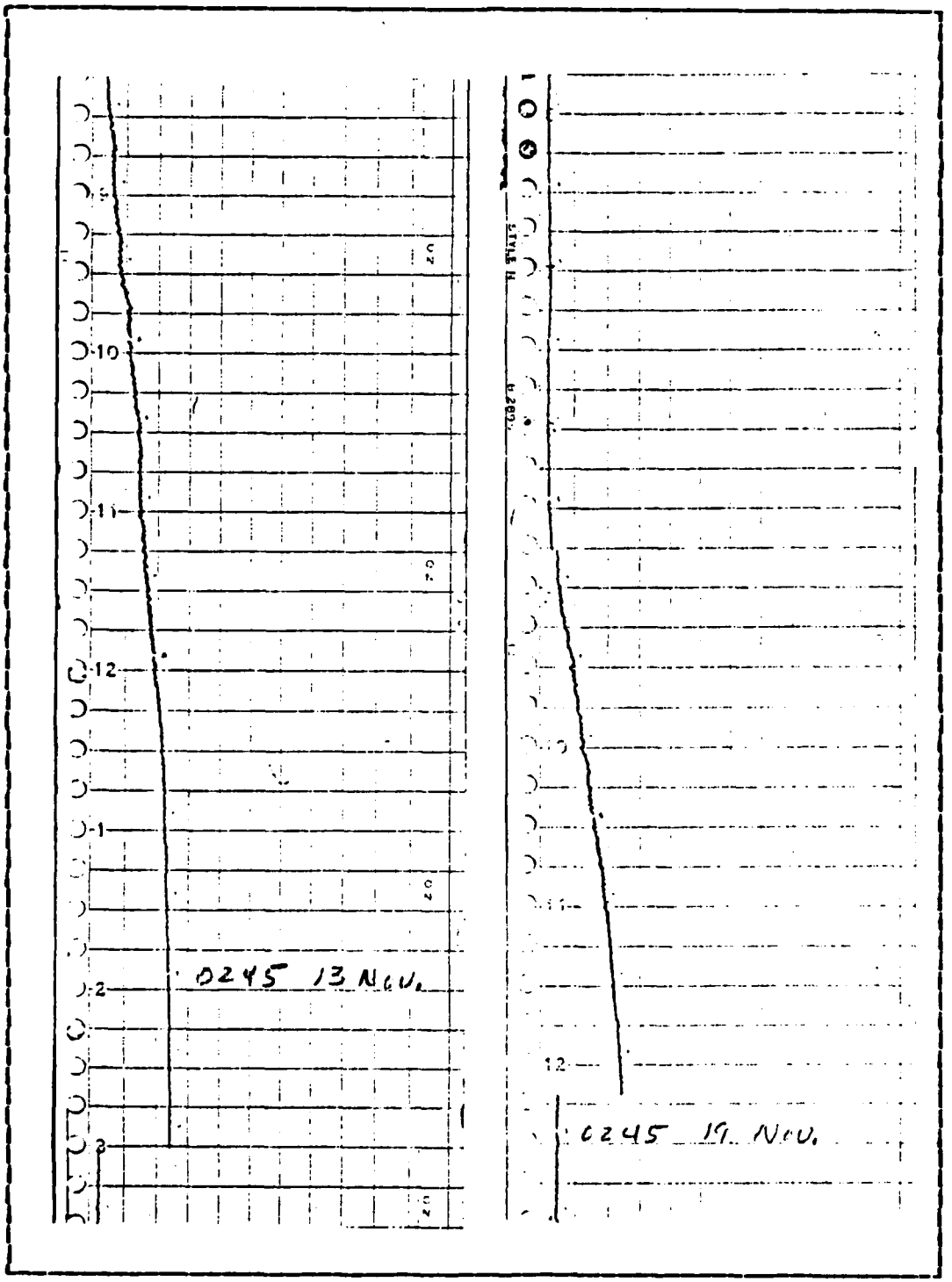

Figure C.2 Channel 7 Recordings

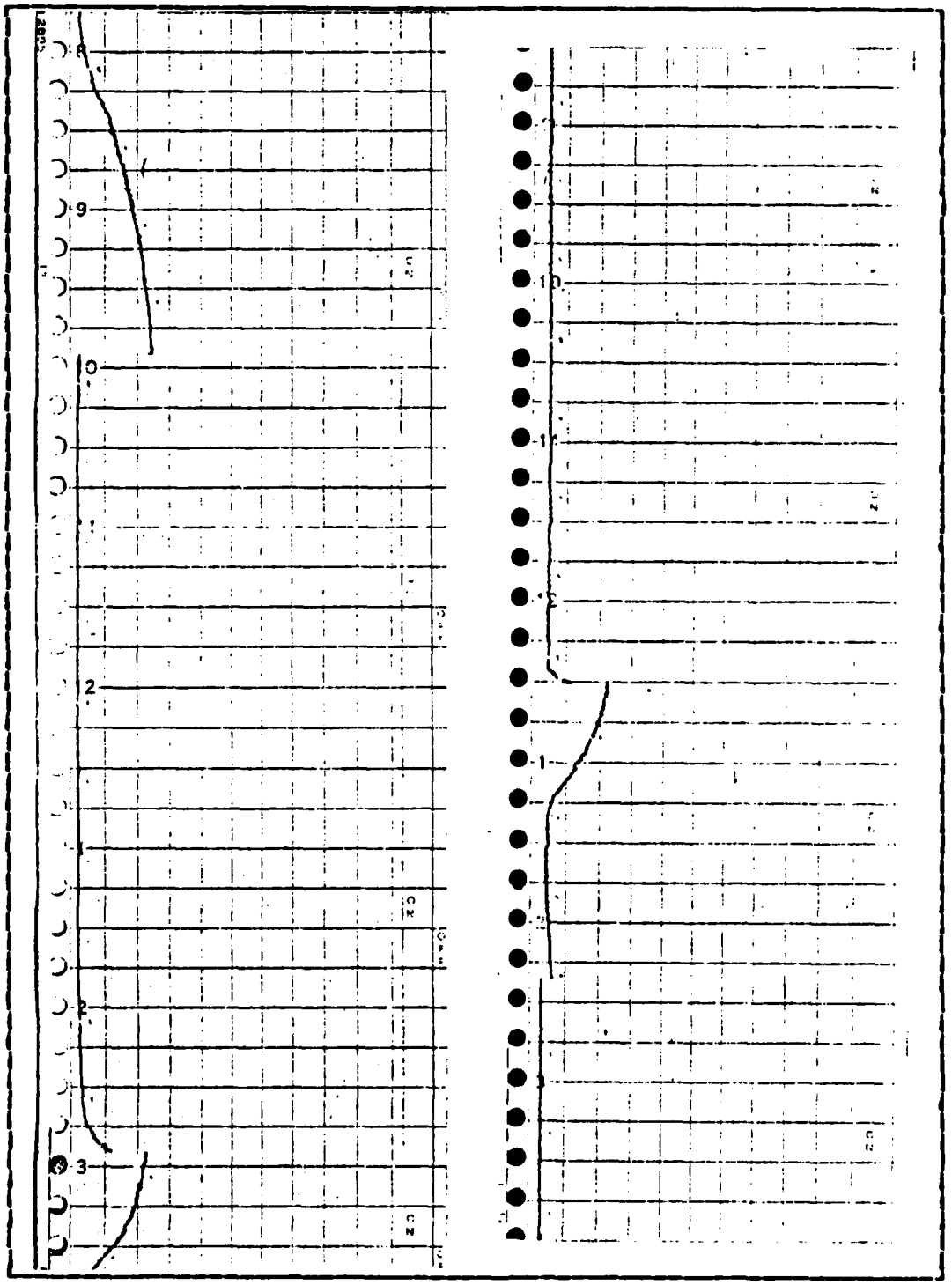

Figure C.3 Channel 7 Recordings

APPENDIX D

PHOTOGRAPHS OF DATA COLLECTION SYSTEM

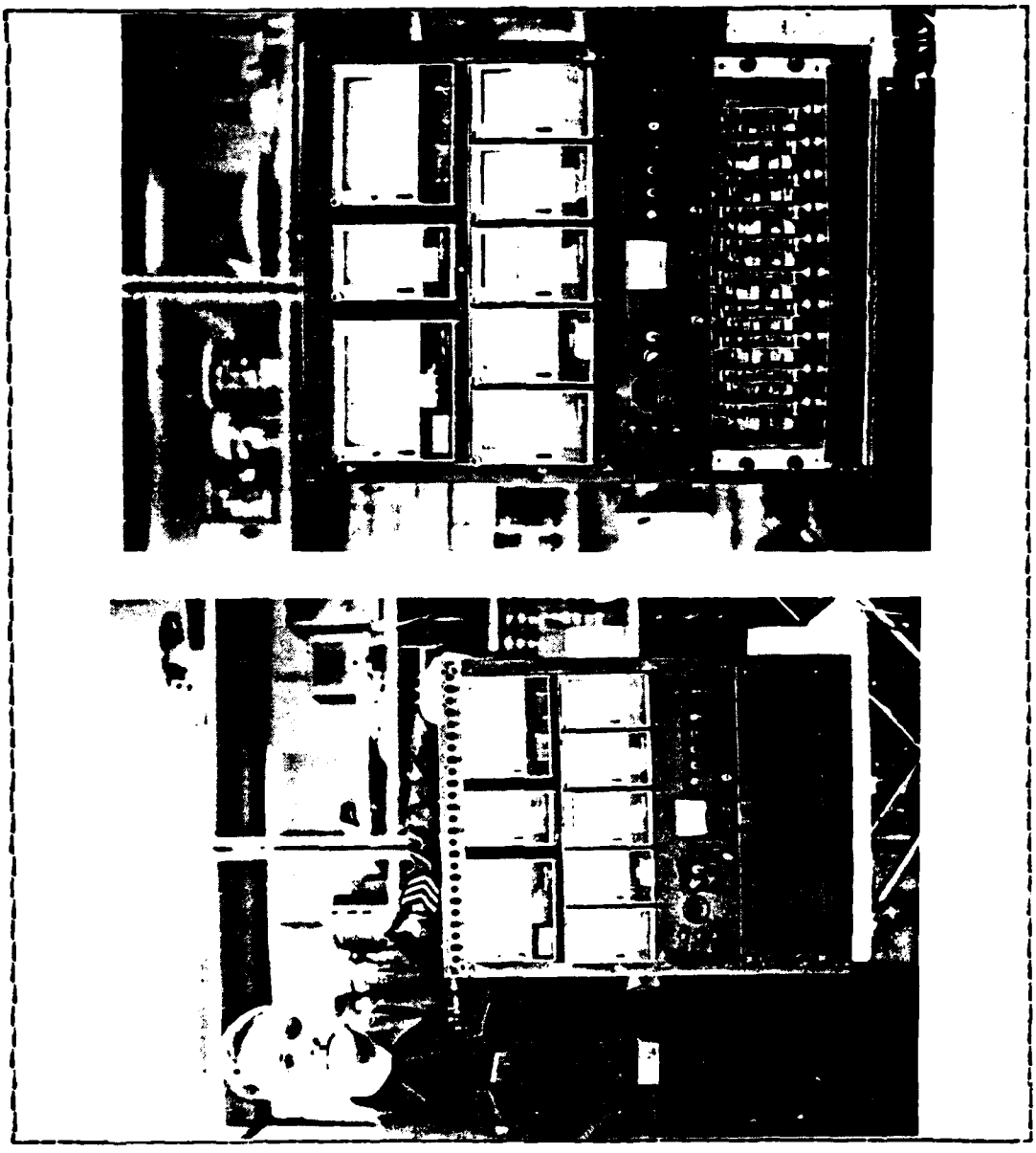

Figure D.1 ET1 Babka and Recorder System

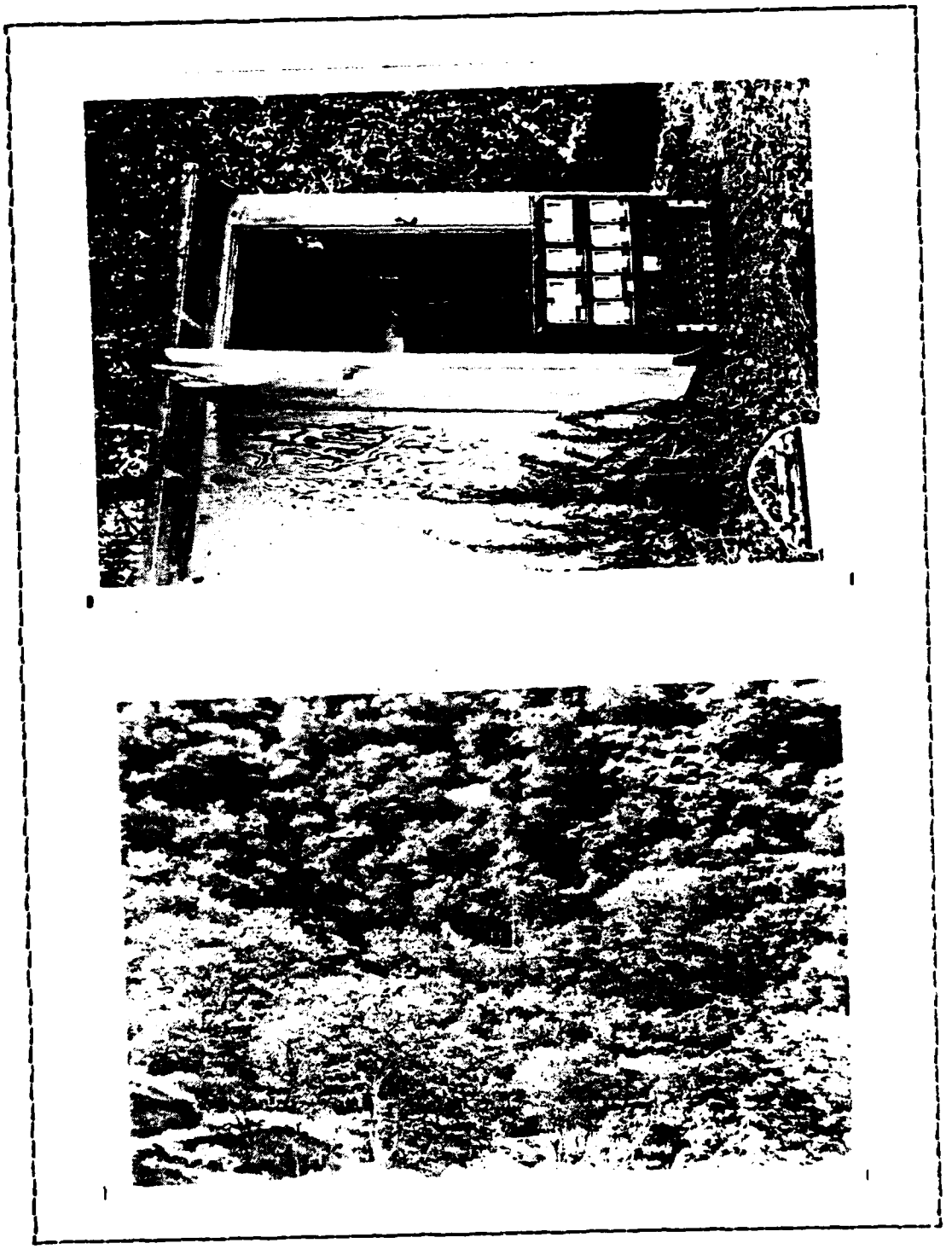

Figure D.2 Antenna Site and Protective Building

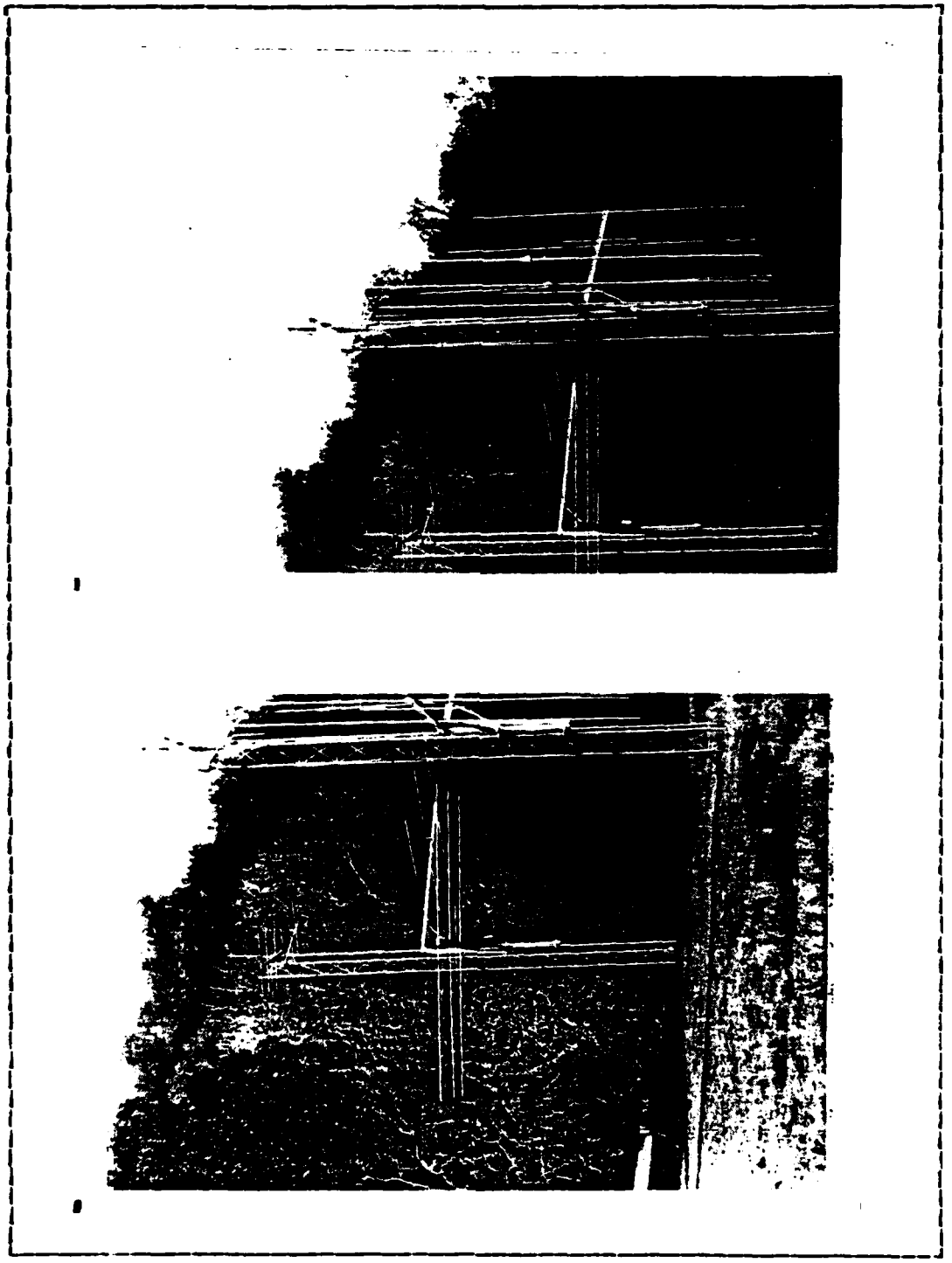

Figure D.3 Antennas and Towers

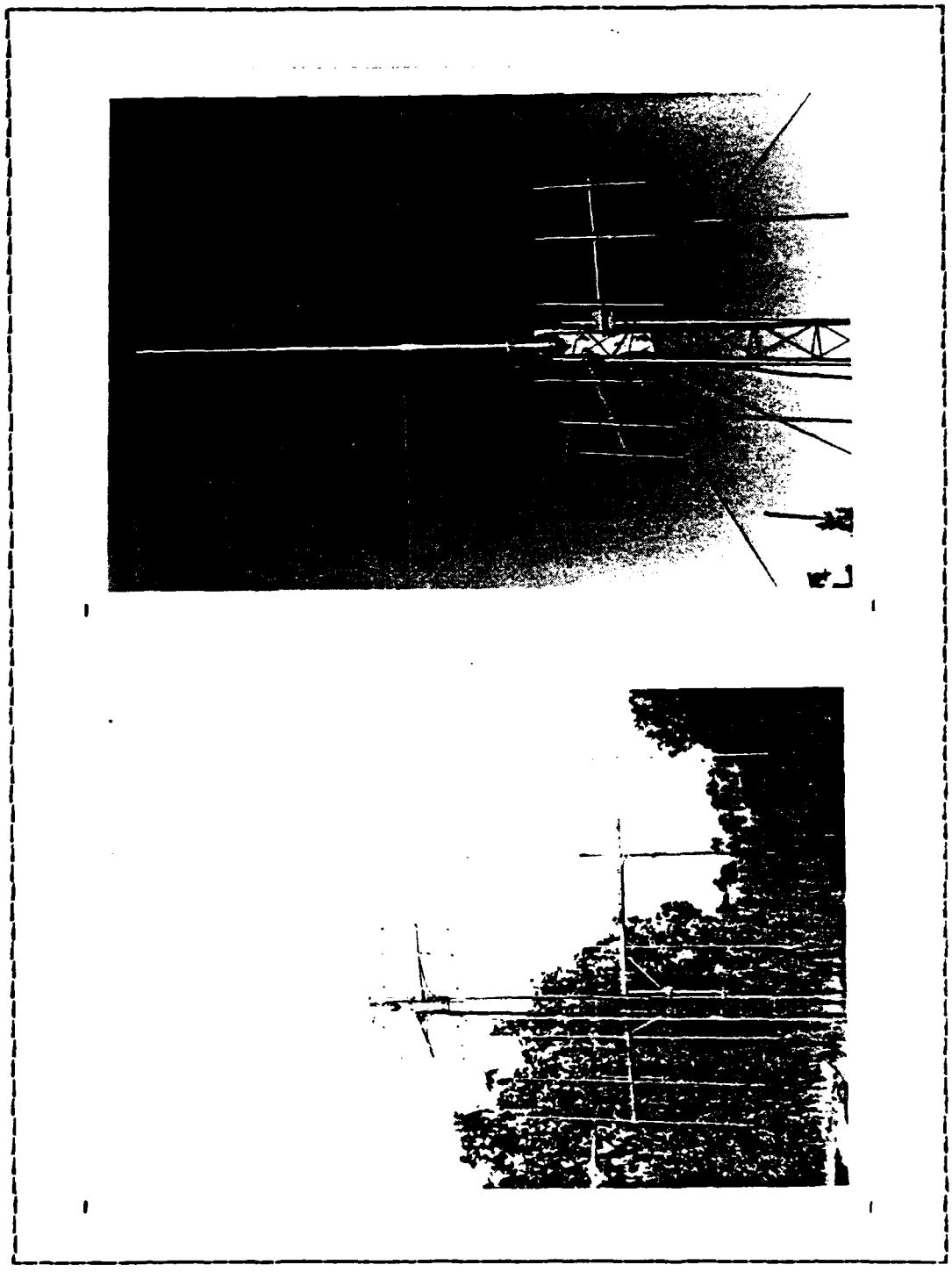

Figure D.4 Antennas and Towers

LIST OF REFERENCES

1. Wesson, Robert L. and Wallace, Robert E., "Predicting the Next Great Earthquake in California," Scientific American, v. 252 number 2, pp. 35-43, February 1985

2. Anderson, Don L. and Dziewonski, Adam M., "Seismic Tomography," Scientific American, v. 251 number 4, pp. 60-68, October 1984

3. Gokhberg, M. B., Morgounov, V. A., Yoshino, T. and Tomizawa, I., "Experimental Measurement of Electromagnetic Emissions Possibly Related to Earthquakes in Japan," Journal of Geophysical Research, v. 87 number B9, pp. 7824-7828, 10 September 1982

4. Derr, J. S., "Earthquake Lights: A Review of Observations and Present Theories," Bull. Seismological Society of America, v. 63, pp. 2177-2187, 1973

5. Warwick, J., Stocker, C., and Meyer, T., "Radio Emission Associated With Rock Fracture: Possible Application to the Great Chilean Earthquake of May 22, 1960," Journal of Geophysical Research, v. 87 number B4, April 1982

6. Ross, M. V., Design of a Freestanding Noise Measurement and Recording System to Predict the Intensity and Location of Electromagnetic Radiation From Earthquakes, Master's Thesis, Naval Postgraduate School, Monterey, California, December 1984

7. Fuhs, A. E., AE-3791 class notes, Naval Postgraduate School, Monterey, California, 1984

8. National Bureau of Standards Technical Note 688, Yagi Antenna Design, by Peter P. Viezbicke, pp.7,9,20, December 1976

9. Radecki, J. T., Spacecraft Power, paper presented at Naval Space Symposium by Hughes Aircraft, Naval Postgraduate School, Monterey CA., 28-30 March 1984

10. Quaglione, G.,"Evolution of the Intelsat System from Intelsat IV to Intelsat V", J. Spacecraft, v. 17 number 2, pp. 67-74, March-April 1980

11. Selby, S. M., Standard Mathematical Tables, edition 20, p. 4, Chemical Rubber Company, 1972

INITIAL DISTRIBUTION LIST

No.		Copies
1.	Library, Code 0142 Naval Postgraduate School Monterey, California 93943-5002	2
2.	Dr. Richard W. Adler Code 62AB Naval Postgraduate School Monterey, California 93943-5004	6
3.	Dr. Stephen Jauregui, Jr. Code 62JA Naval Postgraduate School Monterey, California 93943-5004	1
4.	Defense Technical Information Center Cameron Station Alexandria, Virginia 22304-6145	2
5.	LT Mickey V. Ross 12 Ross Circle North Little Rock, Arkansas 72114	1
6.	CAPT Carl Mortensen MS 977 U. S. Geological Survey 345 Middlefield Menlo Park, California 94025	2
7.	LCDR Michael L. Whyms 276 Second Street Oakfield, Wisconsin 53065	2

END

FILMED

3-86

DTIC